Geochemistry Geophysics Geosystems G3

Article
Volume 14, Number XX
XX Month 2013
doi:10.1002/ggge.20111
ISSN: 1525-2027

Published by AGU and the Geochemical Society

Geochemical insight into differences in the physical structures and dynamics of two adjacent maar lakes at Mt. Vulture volcano (southern Italy)

A. Caracausi, P. M. Nuccio, and R. Favara
Istituto Nazionale di Geofisica e Vulcanologia, Sezione di Palermo, Palermo, Italy (a.caracausi@pa.ingv.it)

M. Nicolosi and A. Rosciglione
Dipartimento di Chimica e Fisica della Terra, Università degli studi di Palermo, Palermo, Italy

M. Paternoster
Dipartimento di Scienze, Università della Basilicata, Potenza, Italy

[1] We report on the first geochemical investigation of the Monticchio maar lakes (Mt. Vulture volcano, southern Italy) covering an annual cycle that aimed at understanding the characteristic features of the physical structures and dynamics of the two lakes. We provide the first detailed description of the lakes based on high-resolution conductivity-temperature-depth (CTD) profiles, chemical and isotopic (H and O) compositions of the water, and the amounts of dissolved gases (e.g., He, Ar, CH_4, and CO_2). The combined data set reveals that the two lakes, which are separated by less than 200 m, exhibit different dynamics: one is a meromictic lake, where the waters are rich in biogenic and mantle-derived gases, while the other is a monomictic lake, which exhibits complete turnover of the water in winter and the release of dissolved gases. Our data strongly suggest that the differences in the dynamics of the two lakes are due to different density profiles affected by dissolved solutes, mainly Fe, which is strongly enriched in the deep water of the meromictic lake. A conceptual model of water balance was constructed based on the correlation between the chemical composition of the water and the hydrogen isotopic signature. Gas-rich groundwaters that feed both of the lakes and evaporation processes subsequently modify the water chemistry of the lakes. Our data highlight that no further potential hazardous accumulation of lethal gases is expected at the Monticchio lakes. Nevertheless, geochemical monitoring is needed to prevent the possibility of vigorous gas releases that have previously occurred in historical time.

Components: 15,500 words, 10 figures, 3 tables.

Keywords: geochemistry; limnology; noble gases; maar lakes.

Index Terms: 1009 Geochemical modeling (3610, 8410); 1845 Limnology (0458, 4239, 4942); 1041 Stable isotope geochemistry (0454, 4870); 8430 Volcanic gases.

Received 18 December 2012; **Revised** 5 March 2013; **Accepted** 7 March 2013

Caracausi, A., M. Nicolosi, P. M. Nuccio, R. Favara, M. Paternoster, and A. Rosciglione (2013), Geochemical insight into differences in the physical structures and dynamics of two adjacent maar lakes at Mt. Vulture volcano (southern Italy), *Geochem. Geophys. Geosyst.*, *14*, doi:10.1002/ggge.20111.

1. Introduction

[2] The release of lethal gases that occurred at Lake Monoun and Lake Nyos in Cameroon on 15 August 1984 and 21 August 1986, respectively, revealed the insidious characteristic of crater lakes being able to suddenly release large amounts of CO_2 stored in their waters [*Kusakabe et al.*, 2000, and references therein]. Several subsequent studies have focused on establishing the processes responsible for these catastrophic events and the triggering mechanism of lethal gas releases [e.g., *Kling*, 1987; *Kling et al.*, 1987; *Sano et al.*, 1987, 1990; *Giggenbach*, 1990; *Kusakabe et al.*, 2008]. Moreover, they have highlighted the gas-rich nature of lakes located near active faults and/or volcanoes.

[3] The hazardous nature of crater lakes has prompted investigations in Earth and environmental sciences aimed at evaluating and possibly mitigating lake gas hazards and limnic explosions. Nevertheless, a review of the recent literature indicates that only a few crater lakes have ever been monitored on a regular basis [*Delmelle and Bernard*, 2000; *Gunkel et al.*, 2008; *Kusakabe et al.*, 2008]. Moreover, lakes situated in volcanic areas that are no longer active have been also investigated in order to evaluate the He flux from subcontinental mantle [e.g., *Giggenbach*, 1990; *Igarashi et al.*, 1992; *Aeschbach-Hertig et al.*, 1996; *Nagao et al.*, 2010], make paleoclimatic reconstructions [e.g., *Allen et al.*, 1999], understand lake ecosystems, and estimate the origin, accumulation, and subsequently transfer to atmosphere of greenhouse gases (mainly CO_2 and CH_4) [e.g., *Assayag et al.*, 2008; *Pasche et al.*, 2011]. Such investigations can take a multidisciplinary approach, where geochemical tools were integrated with classical limnology to better constrain processes governing lake dynamics. Since a volcanic lake collects magmatic and/or hydrothermal gases, its capacity for gas accumulation is controlled by its physical structure and dynamics.

[4] Here we describe the characteristics of two Italian lakes, Lago Piccolo di Monticchio (LPM) and Lago Grande di Monticchio (LGM), which occupy two maar craters that are separated by only 200 m. These lakes are located on Mt. Vulture (southern Italy), a Quaternary volcano that was last active 140 years ago, although its CO_2 degassing level is among the highest in Italy [*Gambardella et al.*, 2004]. The volumes of the lakes were calculated to be 3.98×10^6 m^3 and 3.25×10^6 m^3 for LPM and LGM, respectively, and surfaces of about 1.7×10^5 m^2 and 4.3×10^5 m^2 for LPM and LGM [*Caracausi et al.*, 2009]. A 200 m long channel connects the two lakes, through which LPM water flows toward LGM.

[5] Previous geochemical studies performed at LPM have identified the gas-rich nature of its waters and have also evaluated the possibility of a limnic eruption [*Chiodini et al.*, 1997, 2000; *Cioni et al.*, 2006]. In contrast, investigations of LGM have mainly focused on paleoclimatic aspects [*Brauer et al.*, 2000] and the genesis of its sediments [*Schettler and Albéric*, 2008]. *Caracausi et al.* [2009] provided evidences for the gas-rich nature of LGM, although the total amount of dissolved gases is less than in LPM. The isotopic geochemistry indicates a magmatic origin for both CO_2 and He dissolved in both lakes, with the latter displaying $^3He/^4He$ isotopic ratios close to those measured in olivines ejected from the maars during the last eruption of Mt. Vulture [*Martelli et al.*, 2008; *Caracausi et al.*, 2013].

[6] The present study aims to provide a detailed characterization of the physical structures and dynamics of both Monticchio lakes based on electrical conductivity, temperature profiles, and the chemical compositions of water and dissolved gases gathered during 1 year of surveys carried out between September 2008 and September 2009. We used dissolved gases not only as geochemical tracers for investigating the origin of the gases but also as tracers to constrain the dynamics of the lake waters and the injection of groundwater into the lakes. We also developed a conceptual model of water balance based on the chemical and isotopic compositions of the lake waters: the evolution of the stable isotopes and modification of the water chemistry, as functions of the evaporation and groundwaters inflow, were studied in detail, especially focusing on the differences between and similarities of the two lakes.

2. Sampling and Analytical Methods

[7] The physicochemical structures of the Monticchio lakes were studied by means of conductivity-temperature-depth (CTD) profiles during seven field surveys (Figure 1). We used a high-resolution multiparametric probe (Ageotec IM71) equipped with a pH sensor. This temperature probe has accuracy of 0.01°C and resolution of 0.001°C; the accuracy values of the electrical conductivity (EC) and pH sensors are 0.005 mS cm^{-1} and 0.01 units, respectively. The EC and pH sensors were calibrated with a standard buffer solution before measuring each profile. The lateral continuity of the physicochemical parameters was also verified by measuring profiles at

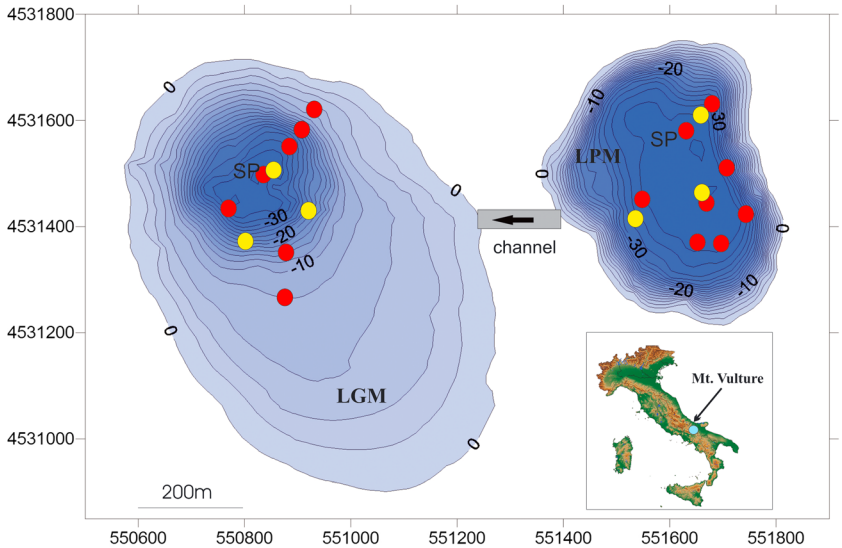

Figure 1. Bathymetric map of the Monticchio lakes showing the sampling points (1 and 2) and CTD profiles used to verify the lateral continuity of physical-chemical parameters (red circles, September 2008; yellow circles, October 2008). SP, sampling point. A 200 m long channel connects the two lakes, through which LPM water flows toward LGM.

several points on each lake (Figure 1). The spatial acquisition step of temperature, EC, and pH data was 1 m.

[8] Water was collected vertically along a water column from the surface down to the bottom at the deepest point of each lake (Figure 1). The water and dissolved-gas samples were collected between September 2008 and September 2009 (listed in Tables 1–3) always at the same point.

[9] The sampling device used to collect the deep lake waters was a 2 L water sampler constructed from clear polycarbonate for determining major and trace elements. The water samples were stored in high-density polyethylene bottles as different aliquots: untreated for δD and $\delta^{18}O$ values, immediately filtered (through a 0.45 μm filter) for anions, and filtered and acidified immediately in the field (with ultrapure HNO_3) for cations. The water samples for trace elements and NH_4^+ were filtered (with a 0.45 μm filter), acidified (with ultrapure HCl) in the field, and stored in polypropylene and dark glass bottles.

[10] The major ions were determined with an ion chromatograph (precision within 5%) using separate columns for cations (Dionex CS-12A Ion Pac for Na^+, K^+, Mg^{2+}, and Ca^{2+}) and anions (Dionex AS14A Ion Pac for F^-, Cl^-, and SO_4^{2-}). Alkalinity was immediately measured by acid titration in the field. Dissolved inorganic carbon (hereafter DIC) values have been calculated by using carbonate equilibrium equations and pH and HCO_3 values. In September 2009, DIC was determined by direct precipitation of total inorganic carbonate (see below for details of the method for the C-isotopic determination of DIC), and HCO_3 was computed by using carbonate equilibrium equations and pH and DIC values. Fe and Mn were determined by ICP Agilent 7500ce with an analytical error of less than 5%. The NH_4^+ content was obtained by a spectrophotometer (Shimatzu UV-VIS) with an analytical error below 0.1 ppm. The ^3H water content [reported in tritium units (TU)] was determined using electrolytic enrichment followed by liquid scintillation counting (the standard deviation varied between ±0.6 and ±1.0 TU depending on the ^3H activity of the water samples). The waters for dissolved-gas analysis were sampled using stainless-steel cylindrical samplers equipped with two pneumatic valves and controlled by a small air compressor [*Cosenza et al.*, 2008; *Caracausi et al.*, 2009]. The concentrations of dissolved He, Ar, O_2, and CH_4 gases and the isotopic composition of Ar were determined in the laboratory after connecting a headspace cylinder to each sampler. The sampled water was equilibrated for 24 h with an initially preevacuated headspace at a known temperature and then subsequently extracted [*Caracausi et al.*, 2009]. The extracted gas was analyzed, and the concentration of each gas extracted was calculated using the ideal-gas law while considering the sampled volume, equilibrium temperature, and water salinity [*Caracausi et al.*, 2009].

[11] The chemical composition of the dissolved gases were determined with a gas chromatograph

Table 1. Chemical Composition of LPM Waters and Isotopic Compositions of H, O, and C

Lake	Depth	Date	Na	K	Mg	Ca	NH_4	Fe	Mn	F	Cl	Br	NO_3	SO_4	HCO_3	DIC	P_{CO2}	$\delta^{13}C$(DIC)	δD	$\delta^{18}O$	^3H(TU)
LGM	−3	8 Sep	34.9	21.1	10.2	25.7	n.a.	<0.1	n.d.	0.8	27.3	b.d.l.	b.d.l.	13.9	198.3	3.5	0.003	n.a.	−17	−0.7	n.a.
LGM	−10	8 Sep	32.4	19.9	9.7	31.1	2.1	n.a.	n.a.	0.8	25.9	b.d.l.	b.d.l.	11.1	213.5	5.5	0.033	n.a.	n.a.	n.a.	n.a.
LGM	−15	8 Sep	31.3	19.2	9.7	34.7	3.2	<0.1	n.a.	0.8	24.8	b.d.l.	b.d.l.	9.6	237.9	10.2	0.136	n.a.	−25	−2.6	n.a.
LGM	−20	8 Sep	31.3	19.6	10.0	35.7	3.3	<0.1	n.a.	0.8	24.1	b.d.l.	b.d.l.	9.1	256.2	19.4	0.242	n.a.	−28	−3.1	n.a.
LGM	−25	8 Sep	31.3	19.6	10.9	40.1	13.4	<0.1	n.a.	0.6	24.1	b.d.l.	b.d.l.	8.2	295.9	27.6	0.367	n.a.	−28	−3.2	n.a.
LGM	−30	8 Sep	31.0	19.9	11.3	41.9	18.4	<0.1	n.a.	0.8	24.1	b.d.l.	b.d.l.	8.7	302.0	28.4	0.374	n.a.	−30	−3.0	n.a.
LGM	−35	8 Sep	31.3	20.3	11.4	42.5	19.5	<0.1	n.a.	0.8	23.8	b.d.l.	b.d.l.	6.7	320.3	16.8	0.367	n.a.	−29	−3.3	n.a.
LGM	−3	8 Oct	34.5	21.1	10.3	27.3	b.d.l.	n.a.	n.a.	1.0	27.7	<0.1	<0.1	13.5	195.2	3.3	0.001	n.a.	−18	−0.7	n.a.
LGM	−10	8 Oct	30.8	19.2	9.2	33.1	0.7	n.a.	n.a.	0.8	25.5	<0.1	<0.1	9.6	204.4	6.1	0.050	n.a.	−25	−2.3	n.a.
LGM	−15	8 Oct	30.4	19.2	9.6	34.7	3.4	n.a.	n.a.	0.8	25.2	<0.1	<0.1	10.1	207.4	11.0	0.147	n.a.	−27	−2.6	n.a.
LGM	−20	8 Oct	30.4	19.6	10.1	37.1	8.7	n.a.	n.a.	0.8	25.2	<0.1	<0.1	10.1	244.0	22.6	0.374	n.a.	−27	−3.0	n.a.
LGM	−25	8 Oct	30.1	19.6	10.7	40.1	14.6	n.a.	n.a.	0.8	24.5	<0.1	<0.1	8.2	286.7	31.5	0.558	n.a.	−30	−3.3	n.a.
LGM	−30	8 Oct	30.1	19.9	10.9	41.3	16.6	n.a.	n.a.	0.8	24.8	<0.1	<0.1	9.1	253.2	27.8	0.509	n.a.	−30	−3.4	n.a.
LGM	−35	8 Oct	30.1	19.9	11.1	42.1	17.7	n.a.	n.a.	0.8	24.8	<0.1	<0.1	6.2	305.0	26.0	0.468	n.a.	−30	−3.4	n.a.
LGM	−3	9 Feb	30.6	19.6	10.1	35.5	b.d.l.	n.a.	n.a.	0.8	25.9	<0.1	1.9	17.3	201.3	5.7	0.040	n.a.	−26	−2.3	2.4
LGM	−10	9 Feb	30.6	19.9	10.2	34.9	b.d.l.	n.a.	n.a.	0.8	25.5	<0.1	1.2	16.8	195.2	6.2	0.050	n.a.	−26	−2.3	n.a.
LGM	−15	9 Feb	30.6	19.9	10.2	35.5	b.d.l.	n.a.	n.a.	0.8	25.5	<0.1	1.2	16.8	201.3	6.7	0.056	n.a.	−26	−2.5	n.a.
LGM	−20	9 Feb	30.6	19.6	10.2	35.7	b.d.l.	n.a.	n.a.	0.8	25.5	<0.1	1.2	16.8	195.2	7.8	0.073	n.a.	−26	−2.5	2.2
LGM	−25	9 Feb	30.6	19.6	10.3	35.1	0.6	n.a.	n.a.	0.8	26.2	<0.1	1.2	16.3	204.4	12.1	0.140	n.a.	−26	−2.4	1.0
LGM	−30	9 Feb	31.0	19.6	10.6	37.9	1.4	n.a.	n.a.	0.8	26.2	<0.1	0.6	16.3	265.4	32.8	0.454	n.a.	−25	−2.6	n.a.
LGM	−35	9 Feb	30.1	19.9	10.6	39.5	9.6	n.a.	n.a.	0.8	25.9	<0.1	0.6	11.5	292.8	26.4	0.301	n.a.	−28	−3.2	1.8
LGM	−3	9 Mar	30.8	19.2	10.0	36.3	n.a.	n.a.	n.a.	0.6	25.5	<0.1	3.1	18.3	207.4	4.2	0.013	n.a.	−28	−3.0	n.a.
LGM	−10	9 Mar	30.4	19.2	10.0	37.1	0.7	n.a.	n.a.	0.6	25.2	<0.1	2.5	17.8	207.4	5.2	0.028	n.a.	−27	−2.8	n.a.
LGM	−15	9 Mar	30.4	19.2	10.1	37.1	1.1	n.a.	n.a.	0.6	25.5	<0.1	2.5	17.3	216.6	6.3	0.042	n.a.	−28	−2.9	n.a.
LGM	−20	9 Mar	30.8	18.8	10.2	36.7	0.9	n.a.	n.a.	0.8	25.9	<0.1	2.5	17.3	201.3	6.1	0.043	n.a.	−25	−2.6	n.a.
LGM	−25	9 Mar	31.3	19.6	10.3	37.1	1.3	n.a.	n.a.	0.8	25.5	<0.1	1.2	17.3	213.5	6.7	0.049	n.a.	−26	−2.6	n.a.
LGM	−30	9 Mar	31.3	19.2	10.5	37.7	1.6	n.a.	n.a.	0.8	26.9	<0.1	3.1	16.8	213.5	6.8	0.051	n.a.	−25	−2.5	n.a.
LGM	−35	9 Mar	31.0	19.6	10.3	36.7	1.6	n.a.	n.a.	0.8	25.9	<0.1	n.a.	14.4	250.1	20.8	0.259	n.a.	−25	−2.7	n.a.
LGM	−3	9 May	30.8	18.8	10.0	38.1	0.2	n.a.	n.a.	0.8	23.4	<0.1	<0.1	19.7	204.4	3.8	0.010	−2.04	−27	−2.9	n.a.
LGM	−10	9 May	31.5	18.8	10.3	38.7	1.6	n.a.	n.a.	0.8	24.1	<0.1	0.6	16.8	216.6	6.5	0.047	−3.66	−28	−2.4	n.a.
LGM	−15	9 May	32.2	19.6	10.5	38.7	2.0	n.a.	n.a.	0.8	24.1	<0.1	<0.1	16.8	231.8	8.0	0.065	−3.71	−25	−2.4	n.a.
LGM	−20	9 May	32.4	19.9	10.5	38.7	2.2	n.a.	n.a.	0.8	24.1	<0.1	<0.1	16.3	228.8	9.4	0.088	−3.25	−26	−2.5	n.a.
LGM	−25	9 May	32.7	19.9	10.6	38.7	2.7	n.a.	n.a.	0.8	24.1	<0.1	<0.1	15.9	225.7	9.9	0.096	−3.00	−25	−2.2	n.a.
LGM	−30	9 May	32.9	19.9	10.7	39.1	3.3	n.a.	n.a.	0.8	24.1	<0.1	<0.1	15.9	228.8	10.5	0.104	−3.53	−27	−2.5	n.a.
LGM	−35	9 May	32.9	19.9	10.6	38.7	3.3	n.a.	n.a.	0.8	24.5	<0.1	<0.1	15.4	250.1	17.8	0.212	−3.11	−27	−2.8	n.a.
LGM	−3	9 Jun	30.8	18.4	9.0	28.3	0.2	n.a.	n.a.	0.8	23.8	<0.1	<0.1	18.7	189.1	3.5	0.009	n.a.	−23	−2.5	n.a.
LGM	−10	9 Jun	29.9	18.8	8.6	37.7	2.0	n.a.	n.a.	0.8	24.1	<0.1	<0.1	15.9	222.7	6.5	0.045	−2.54	−24	−3.1	n.a.
LGM	−15	9 Jun	30.1	18.8	9.0	37.5	2.4	n.a.	n.a.	0.6	24.5	<0.1	0.6	16.3	234.9	7.4	0.056	−2.39	−25	−3.0	n.a.
LGM	−20	9 Jun	30.5	18.8	9.4	37.7	2.5	n.a.	n.a.	0.8	24.5	<0.1	<0.1	15.9	225.7	9.5	0.089	−2.36	−25	−2.9	n.a.
LGM	−25	9 Jun	30.6	19.2	9.6	37.9	3.3	n.a.	n.a.	0.6	24.5	<0.1	<0.1	14.9	231.8	10.9	0.111	−2.72	−24	−2.8	n.a.
LGM	−30	9 Jun	30.8	19.2	9.8	36.9	3.6	n.a.	n.a.	0.8	24.5	<0.1	0.6	14.9	231.8	11.1	0.113	−2.40	−25	−2.9	n.a.
LGM	−35	9 Jun	30.4	18.8	9.8	36.9	4.5	n.a.	n.a.	0.6	23.4	<0.1	0.6	13.9	231.8	19.4	0.241	−2.09	−24	−2.9	n.a.
LGM	−3	9 Sep	36.6	22.3	11.2	32.1	0.2	1.7	<0.1	0.8	26.9	<0.1	<0.1	18.7	175.2	2.9	0.009	−3.43	−19	−0.9	n.a.

LGM	−10	9 Sep	33.8	20.3	10.7	41.1	2.9	0.6	<0.1	0.8	24.8	<0.1	<0.1	15.9	163.5	3.9	0.093	−3.40	−18	−0.7	n.a.
LGM	−15	9 Sep	33.6	19.9	10.7	40.3	3.1	0.6	<0.1	0.8	25.2	<0.1	<0.1	15.9	156.2	4.1	0.137	−3.87	−27	−2.9	n.a.
LGM	−20	9 Sep	33.8	20.3	10.8	40.1	4.2	0.8	<0.1	0.8	25.5	<0.1	<0.1	14.9	154.3	4.6	0.254	−4.21	−27	−2.7	n.a.
LGM	−25	9 Sep	33.3	20.3	10.8	39.9	4.9	1.1	<0.1	0.8	25.5	<0.1	<0.1	14.4	148.8	4.9	0.304	−2.94	−27	−2.8	n.a.
LGM	−30	9 Sep	33.6	20.3	10.8	39.9	5.1	1.4	<0.1	0.8	25.5	<0.1	<0.1	14.9	154.9	5.2	0.310	−2.76	−26	−2.4	n.a.
LGM	−35	9 Sep	33.6	20.3	10.8	40.7	5.1	1.4	<0.1	0.8	23.8	0.8	<0.1	13.9	166.5	6.3	0.494	−2.43	−26	−2.6	n.a.

Ion concentrations are in mg kg^{-1}; DIC and P_{CO2} values are in mol L^{-1} and atm, respectively; δD and $\delta^{18}O$ values are per mil versus V-SMOW; $\delta^{13}C$ values are per mil versus V-PDB. The tritium value for rain sampled in 2009 using a pluviometer located 3 km from the lakes is 4.0 TU (±1.0); n.a = not available; b.l.d.= below detection limit.

(Perkin Elmer 8500) with Ar carrier gas (and using He for Ar measurements) on a 4 m column (Carbosieve SII) and a double detector (TCD and FID). The detection limits were 500 ppmv. for O_2 and 1 ppmv for CH_4. The analytical error was about ±3% for all species. The abundances of dissolved He were measured in a split-flight-tube mass spectrometer (Helix SFT) equipped with a purification line for separating noble gases from the gaseous mixture [*Nuccio et al.*, 2008]. Ar isotopes were analyzed in a multicollector mass spectrometer (Argus).

[12] The samples for determining the carbon isotopes of total dissolved inorganic carbon (TDIC) were collected using the stainless-steel sampler (for dissolved gases) equipped with two additional ball valves (Swagelok type) and using two syringes to prevent any depressurization during water extraction [*Nicolosi*, 2010; *Cosenza et al.*, 2012]. The forced introduction of water from a ball valve fills the syringe connected at the other valve with lake water (due to the piston effect). The latter syringe contained an alkaline solution of $SrCl_2$ and NaOH at pH≈13; therefore, as the sampled lake water was transferred into the syringe, all of the DIC precipitated as $SrCO_3$ [*Bishop*, 1990; *Kusakabe et al.*, 1990; *Nojiri et al.*, 1993; *Kusakabe et al.*, 2000; *Zhang et al.*, 2009]. The precipitate was filtered and dried and then analyzed for isotopic compositions of carbon. Carbon isotopic ratios were measured with a mass spectrometer (Finnigan Delta-S).

[13] The D/H isotopic ratio in the water samples was determined using the Zn-reduction technique described by *Kendall and Coplen* [1985], while $^{18}O/^{16}O$ was analyzed by CO_2-water equilibration techniques [*Epstein and Mayeda*, 1953]. A mass spectrometer (Thermo Delta XP CF) equipped with a peripheral device (TC-EA) and interface (CONFLO III) was used to analyze H. $^{18}O/^{16}O$ ratios were measured by mass spectrometry (AP 2003 CF-IRMS).

[14] The isotope results are reported in δ per mil units versus the Vienna SMOW (V-SMOW) standard for H and O and versus the Vienna Pee Dee belemnite (V-PDB) standard for carbon. The standard deviation of the measurements was about ±1‰ for δD and ±0.2‰ for $\delta^{18}O$ and $\delta^{13}C$.

[15] All sampling and analytical devices were provided by the Istituto Nazionale di Geofisica e Vulcanologia, Sezione di Palermo. Tritium was analyzed in the laboratories of Instituto Tecnológico e Nuclear of Sacavém (Portugal).

Table 2. Chemical Composition of LGM Waters and Isotopic Compositions of H, O, and C

Lake	Depth	Date	Na	K	Mg	Ca	NH_4	Fe	Mn	F	Cl	Br	NO_3	SO_4	HCO_3	DIC	P_{CO2}	$\delta^{13}C$(DIC)	δD	$\delta^{18}O$	^3H(TU)
LPM	−3	8 Sep	32.0	21.1	14.6	22.85	<0.01	<0.01	<0.01	1.0	19.9	b.d.l.	b.d.l.	8.2	183.0	3.1	0.002	n.a.	n.a.	n.a.	n.a.
LPM	−12	8 Sep	31.0	20.7	14.3	22.44	<0.01	<0.01	<0.01	1.0	18.8	b.d.l.	b.d.l.	7.7	176.9	4.1	0.020	n.a.	−39	−5.2	n.a.
LPM	−18	8 Sep	34.0	22.7	19.2	30.06	9.5	106.8	1.9	0.6	23.4	b.d.l.	b.d.l.	4.8	335.5	14.5	0.143	n.a.	−44	−6.1	n.a.
LPM	−25	8 Sep	37.7	25.0	25.0	37.27	14.0	124.5	1.9	0.6	19.9	b.d.l.	b.d.l.	1.4	542.9	22.9	0.242	n.a.	−51	−8.0	n.a.
LPM	−28	8 Sep	37.2	25.4	25.8	38.48	15.3	122.2	1.9	0.6	20.2	b.d.l.	b.d.l.	1.4	497.2	21.0	0.221	–	−52	−7.9	n.a.
LPM	−32	8 Sep	38.6	25.8	27.2	40.08	14.0	112.1	1.5	0.6	20.6	b.d.l.	b.d.l.	1.9	588.7	24.6	0.259	n.a.	−52	−8.1	n.a.
LPM	−36.5	8 Sep	38.6	26.2	28.3	41.48	21.4	258.9	2.5	0.6	20.6	0.8	b.d.l	2.4	661.9	26.3	0.279	n.a.	−53	−8.3	n.a.
LPM	−3	8 Oct	31.5	21.1	14.3	22.44	24.7	n.a.	n.a.	1.0	20.2	b.d.l.	b.d.l.	8.7	n.a.	n.a.	n.a.	n.a.	−35	−4.1	n.a.
LPM	−12	8 Oct	30.6	20.7	14.3	22.44	24.0	n.a.	n.a.	1.0	19.5	b.d.l.	b.d.l.	7.7	n.a.	n.a.	n.a.	n.a.	−39	−4.8	n.a.
LPM	−18	8 Oct	34.3	22.7	22.3	32.46	26.9	n.a.	n.a.	0.8	17.4	b.d.l.	b.d.l.	2.9	n.a.	n.a.	n.a.	n.a.	−49	−7.2	n.a.
LPM	−25	8 Oct	35.4	23.8	25.0	35.87	27.8	n.a.	n.a.	0.6	17.7	b.d.l.	b.d.l.	1.4	n.a.	n.a.	n.a.	n.a.	−53	−8.1	n.a.
LPM	−28	8 Oct	35.6	23.8	25.8	36.07	28.0	n.a.	n.a.	0.6	17.7	b.d.l.	b.d.l.	1.4	n.a.	n.a.	n.a.	n.a.	−53	−8.3	n.a.
LPM	−32	8 Oct	36.8	24.6	26.1	37.68	28.9	n.a.	n.a.	0.6	18.1	b.d.l.	b.d.l.	1.4	n.a.	n.a.	n.a.	n.a.	−54	−8.2	n.a.
LPM	−36.5	8 Oct	36.1	24.2	27.5	38.88	28.3	n.a.	n.a.	0.6	16.3	b.d.l.	b.d.l.	1.9	n.a.	n.a.	n.a.	n.a.	−53	−8.4	n.a.
LPM	−3	9 Feb	29.9	20.7	14.3	23.05	<0.01	n.a.	n.a.	0.8	19.5	b.d.l.	0.6	8.2	n.a.	n.a.	n.a.	n.a.	−38	−4.9	0.6
LPM	−12	9 Feb	29.7	20.7	14.0	22.24	<0.01	n.a.	n.a.	0.8	19.9	b.d.l.	0.6	8.2	n.a.	n.a.	n.a.	n.a.	−40	−4.9	n.a.
LPM	−18	9 Feb	32.4	23.1	19.5	30.06	1.6	n.a.	n.a.	0.8	19.1	b.d.l.	b.d.l.	3.4	n.a.	n.a.	n.a.	n.a.	−46	−6.8	n.a.
LPM	−25	9 Feb	35.4	25.0	24.2	36.47	9.4	n.a.	n.a.	0.6	20.6	b.d.l.	1.2	1.0	n.a.	n.a.	n.a.	n.a.	−52	−8.1	−1.4
LPM	−28	9 Feb	36.1	24.6	25.3	38.48	12.1	n.a.	n.a.	0.6	20.6	b.d.l.	b.d.l.	0.5	n.a.	n.a.	n.a.	n.a.	−53	−8.4	0.0
LPM	−32	9 Feb	36.1	25.4	25.8	38.88	14.6	n.a.	n.a.	0.6	18.8	b.d.l.	b.d.l.	0.5	n.a.	n.a.	n.a.	n.a.	−53	−8.4	n.a.
LPM	−36.5	9 Feb	36.6	25.8	26.9	43.09	23.5	n.a.	n.a.	0.6	19.5	b.d.l	b.d.l.	0.5	n.a.	n.a.	n.a.	n.a.	−54	−8.4	0.0
LPM	−3	9 Mar	30.4	20.3	13.5	21.44	n.a.	n.a.	n.a.	1.0	19.1	b.d.l.	0.6	7.7	164.7	3.3	0.010	n.a.	−38	−5.2	n.a.
LPM	−12	9 Mar	30.4	20.3	13.7	21.64	0.2	n.a.	n.a.	1.0	19.1	b.d.l.	0.6	7.7	173.9	3.7	0.014	n.a.	−36	−5.3	n.a.
LPM	−18	9 Mar	30.4	20.3	13.7	21.64	0.4	n.a.	n.a.	1.0	19.1	b.d.l.	0.6	7.7	n.a.	n.a.	n.a.	n.a.	−45	−5.3	n.a.
LPM	−25	9 Mar	34.0	23.5	19.8	30.66	8.1	n.a.	n.a.	0.8	20.2	b.d.l.	b.d.l.	3.4	539.9	30.8	0.379	n.a.	−51	−7.0	n.a.
LPM	−28	9 Mar	37.2	25.4	24.5	37.07	16.1	n.a.	n.a.	0.6	20.2	b.d.l.	0.6	1.0	564.3	31.1	0.379	n.a.	−51	−8.4	n.a.
LPM	−32	9 Mar	37.2	25.0	24.7	37.68	13.9	n.a.	n.a.	0.6	20.6	b.d.l.	b.d.l.	1.0	625.3	33.2	0.398	n.a.	−51	−8.2	n.a.
LPM	−36.5	9 Mar	37.2	25.4	26.4	39.28	16.4	n.a.	n.a.	0.6	19.9	b.d.l.	b.d.l.	1.4	738.1	37.7	0.461	n.a.	−52	−8.4	n.a.
LPM	−3	9 May	29.2	19.6	13.5	21.84	<0.01	n.a.	n.a.	0.8	18.4	b.d.l.	b.d.l.	7.7	164.7	2.8	0.001	−3.21	−38	−5.1	n.a.
LPM	−12	9 May	30.4	19.9	13.7	21.64	0.2	n.a.	n.a.	1.0	19.1	b.d.l.	0.6	7.7	170.8	4.8	0.031	−5.16	−38	−5.0	n.a.
LPM	−18	9 May	35.4	23.5	19.5	30.66	7.6	n.a.	n.a.	0.6	19.1	b.d.l.	0.6	2.9	305.0	24.1	0.318	−2.85	−39	−6.7	n.a.
LPM	−25	9 May	38.4	25.4	24.5	37.68	14.3	n.a.	n.a.	0.6	19.9	b.d.l.	b.d.l.	1.0	549.0	41.3	0.560	−1.87	−46	−8.1	n.a.
LPM	−28	9 May	39.1	25.8	25.6	38.68	15.9	n.a.	n.a.	0.6	19.9	b.d.l.	b.d.l.	1.0	536.8	38.9	0.521	−1.37	−51	−8.2	n.a.
LPM	−32	9 May	40.7	26.6	27.2	40.48	15.5	n.a.	n.a.	0.6	19.5	b.d.l.	b.d.l.	1.0	555.1	39.9	0.555	−1.03	−51	−8.2	n.a.
LPM	−36.5	9 May	41.8	28.2	26.9	45.69	23.1	n.a.	n.a.	0.6	19.5	b.d.l	0.6	1.0	671.0	40.3	0.539	−0.21	−50	−8.7	n.a.
LPM	−3	9 Jun	31.5	20.7	12.9	22.65	<0.01	n.a.	n.a.	1.0	19.1	b.d.l.	b.d.l.	8.2	173.9	2.9	0.001	−3.35	−34	−4.7	n.a.
LPM	−12	9 Jun	32.0	21.1	14.3	23.85	0.2	n.a.	n.a.	1.0	19.1	b.d.l.	0.6	7.78	183.0	4.7	0.033	−3.75	−39	−5.3	n.a.
LPM	−18	9 Jun	31.0	20.7	16.5	28.26	7.6	n.a.	n.a.	0.8	18.8	b.d.l.	b.d.l.	2.9	271.5	17.8	0.220	−2.82	−46	−6.9	n.a.
LPM	−25	9 Jun	34.5	22.7	22.5	35.47	14.8	n.a.	n.a.	0.6	19.1	b.d.l.	b.d.l.	0.5	524.6	33.3	0.429	−2.25	−53	−8.5	n.a.
LPM	−28	9 Jun	35.4	23.5	24.2	37.07	15.7	n.a.	n.a.	0.6	19.1	b.d.l.	0.6	0.5	533.8	33.8	0.449	n.a.	−53	−8.7	n.a.
LPM	−32	9 Jun	35.2	23.5	25.0	40.28	21.3	n.a.	n.a.	0.6	18.8	b.d.l.	0.6	1.0	603.9	36.5	0.480	−1.86	−54	−8.7	n.a.
LPM	−36.5	9 Jun	36.3	24.2	26.9	44.69	27.8	n.a.	n.a.	0.6	19.5	b.d.l.	3.1	1.4	750.3	38.2	0.467	−0.40	−52	−8.7	n.a.
LPM	−3	9 Sep	33.8	22.3	14.8	23.05	26.6	<0.01	<0.01	1.0	19.5	<0.01	b.d.l.	8.7	196.4	3.3	0.001	−3.01	−34	−4.3	n.a.

LPM	−12	9 Sep	32.9	21.5	15.1	23.65	25.8	<0.01	0.3	1.0	19.5	<0.01	b.d.l.	8.2	118.3	3.0	0.018	−2.84	−34	−4.2	n.a.
LPM	−18	9 Sep	40.0	26.2	24.2	38.28	31.4	106.3	1.9	0.8	19.1	<0.01	b.d.l.	7.7	93.9	5.9	0.072	−4.13	−39	−5.4	n.a.
LPM	−25	9 Sep	40.7	26.6	25.6	40.28	31.9	117.8	1.9	0.6	20.6	<0.01	b.d.l.	0.5	212.3	13.1	0.167	−1.86	−51	−8.2	n.a.
LPM	−28	9 Sep	40.9	26.6	25.8	41.08	32.1	123.1	1.9	0.6	21.3	<0.01	b.d.l.	0.5	244.6	14.8	0.187	−2.08	−53	−8.5	n.a.
LPM	−32	9 Sep	40.9	27.8	26.9	43.89	32.1	150.5	1.9	0.6	20.9	<0.01	b.d.l.	0.5	302.0	17.9	0.224	−1.46	−53	−8.5	n.a.
LPM	−36.5	9 Sep	42.3	29.7	29.1	51.70	33.2	243.6	2.5	0.6	19.5	<0.01	b.d.l.	0.5	311.1	23.1	0.324	0.13	−54	−8.5	n.a.
Channel		9 Feb	29.9	20.7	14.0	22.24	n.a.	n.a.	n.a.	1.0	19.1	<0.01	b.d.l.	7.7	n.a.	n.a.	n.a.	n.a.	−38	−4.9	n.a.
Channel 1		9 Mar	30.8	20.7	14.6	23.25	n.a.	n.a.	n.a.	1.0	19.5	<0.01	0.6	8.7	n.a.	n.a.	n.a.	n.a.	n.a.	n.a.	n.a.
Channel 2		9 Mar	30.4	18.8	23.1	37.88	n.a.	n.a.	n.a.	0.6	24.8	<0.01	2.5	19.7	n.a.	n.a.	n.a.	n.a.	n.a.	n.a.	n.a.
Channel		9 Jun	30.6	20.3	13.7	22.65	n.a.	n.a.	n.a.	0.8	18.8	<0.01	b.d.l.	7.7	n.a.	n.a.	n.a.	n.a.	−38	−4.4	n.a.
CLG		9 Feb	30.6	19.6	22.5	35.27	n.a.	n.a.	n.a.	0.8	25.5	<0.01	1.9	19.7	n.a.	n.a.	n.a.	n.a.	−27	−2.6	n.a.
CLG		9 Mar	30.8	20.7	16.8	27.05	n.a.	n.a.	n.a.	0.8	19.5	<0.01	0.6	24.5	n.a.	n.a.	n.a.	n.a.	n.a.	n.a.	n.a.

Chemical compositions in ppm. TDIC in mmol/L, P_{CO2} in atm.
Ion concentrations are in mg kg^{-1}; DIC and P_{CO2} values are in mol l^{-1} and atm, respectively; δD and δ^{18}O values are per mil versus V-SMOW; δ^{13}C values are per mil versus V-PDB; n.a. : not available; b.d.l. = below detection limit.

3. Results

3.1. CTD Profiles Along the Water Columns of the Monticchio Lakes

[16] The physical-chemical parameters and chemistry along the water column of both lakes have never been previously investigated on a long-term basis, except for 1 year of monthly temperature measurements at different depths in both lakes [*Zito and Mongelli*, 1980].

[17] A typical seasonal thermal stratification in the epilimnion, metalimnion, and hypolimnion was clearly distinguished in both lakes during the warm period (Figures 2a and 2c). The epilimnion exhibits a seasonally variable temperature associated with a change in the metalimnion thickness. The temperature profiles indicated that the LPM water column is stratified during the warm period into four depth intervals: (I) the upper stratum, from the surface down to about 14 m, shows major seasonal variations of temperature; (II) the metalimnion has an upper boundary that varies over time and a lower one at a depth of around 16 m; (III) between depths of 16 and 30 m lies a zone where temperature increases toward the bottom, although its profile shows small variations over time; and (IV) the bottom zone having a quite stable temperature field with a clear gradient, denoting that these waters have a steady state heat balance (Figure 2b), and according to *Caracausi et al*. [2009, and references therein], such data indicate a heat flow from the lake bottom.

[18] During the warm period, the water column of LGM is thermally divided into three regions: an epilimnion, and a deep hypolimnion separated from the epilimnion by a metalimnion whose thickness varies over time. The latter is thickest during summer and thinnest during winter. In contrast to LPM, the temperature did not increase toward the bottom of LGM.

[19] The EC profiles recorded during the same period show different features at LPM and LGM (Figures 2d and 2e). Four layers have been distinguished for LPM: (I) a shallower layer that extends from the surface to a depth of 14 m and is characterized by seasonal variation of the EC; (II) the chemolimnion, a layer between depths of about 14 and 16 m, where EC strongly increases from 0.4 to 0.9 mS cm^{-1} in response to a change in the chemical composition of water (Table 2); (III) a layer between depths of 16 and 30 m, characterized by a weak increase in EC up to 1.0 mS cm^{-1}; and

Table 3. Chemical Composition of Dissolved Gases in LPM and LGM Waters and the Isotopic Composition of Dissolved Ar

Lake	Depth	Date	He	Ar	O_2	CH_4	$^{40}Ar/^{36}Ar$	Lake	Depth	Date	He	Ar	O_2	CH_4	$^{40}Ar/^{36}Ar$
LGM	−3	8 Sep	6.5E−4	n.a.	2.13	0.04		LPM	−3	8 Sep	n.a.	n.a.	n.a.	n.a.	
LGM	−10	8 Sep	5.6E−4	n.a.	0.23	3.88		LPM	−12	8 Sep	n.a.	n.a.	0.26	0.06	
LGM	−15	8 Sep	7.1E−4	0.29	0.22	7.28		LPM	−18	8 Sep	2.1E−4	0.25	0.10	54.10	
LGM	−20	8 Sep	1.8E−3	0.29	0.13	24.79		LPM	−25	8 Sep	1.5E−3	0.26	0.13	73.73	
LGM	−25	8 Sep	1.9E−3	0.28	0.16	34.67		LPM	−28	8 Sep	2.0E−3	0.26	0.08	81.35	
LGM	−30	8 Sep	2.9E−3	0.30	0.13	44.58		LPM	−32	8 Sep	2.0E−3	0.26	0.05	86.74	
LGM	−35	8 Sep	3.0E−3	0.30	0.13	48.58		LPM	−36.5	8 Sep	1.9E−3	0.22	0.03	136.12	
LGM	−3	8 Oct	2.9E−5	n.a.	2.29	0.01		LPM	−3	8 Oct	1.9E−4	n.a.	n.a.	n.a.	
LGM	−10	8 Oct	1.7E−4	n.a.	0.12	3.14		LPM	−12	8 Oct	1.6E−4	n.a.	0.19	0.49	
LGM	−15	8 Oct	6.5E−4	n.a.	0.15	7.31		LPM	−18	8 Oct	8.2E−4	n.a.	0.07	39.78	
LGM	−20	8 Oct	9.3E−4	n.a.	0.16	18.47		LPM	−25	8 Oct	1.5E−3	n.a.	0.11	72.19	
LGM	−25	8 Oct	1.9E−3	n.a.	0.06	35.00		LPM	−28	8 Oct	1.6E−3	n.a.	0.09	78.04	
LGM	−30	8 Oct	1.7E−3	n.a.	0.03	45.58		LPM	−32	8 Oct	1.6E−3	n.a.	0.51	85.74	
LGM	−35	8 Oct	1.7E−3	n.a.	0.06	45.87		LPM	−36.5	8 Oct	1.5E−3	n.a.	0.08	112.54	
LGM	−3	9 Feb	1.2E−4	0.36	1.46	0.01		LPM	−3	9 Feb	8.0E−5	0.34	2.28	0.02	
LGM	−10	9 Feb	1.7E−4	0.35	0.11	0.01		LPM	−12	9 Feb	8.1E−5	0.34	2.52	0.09	
LGM	−15	9 Feb	1.9E−4	0.34	0.19	0.01		LPM	−18	9 Feb	1.0E−3	0.30	0.07	48.65	
LGM	−20	9 Feb	4.1E−4	0.34	0.02	1.10		LPM	−25	9 Feb	1.7E−3	0.27	0.05	82.96	
LGM	−25	9 Feb	4.4E−4	0.33	0.25	5.33		LPM	−28	9 Feb	1.7E−3	0.27	0.07	86.12	
LGM	−30	9 Feb	1.4E−3	0.30	0.09	32.06		LPM	−32	9 Feb	1.63E−3	0.27	0.05	103.27	
LGM	−35	9 Feb	2.2E−3	0.29	0.06	52.04		LPM	−36.5	9 Feb	n.a.	n.a.	n.a.	n.a.	
LGM	−3	9 Mar	5.4E−5	n.a.	1.99	0.00		LPM	−3	9 Mar	6.3E−5	0.30	1.30	0.06	
LGM	−10	9 Mar	7.6E−5	0.26	1.21	0.00		LPM	−12	9 Mar	n.a.	n.a.	n.a.	n.a.	
LGM	−15	9 Mar	1.1E−4	0.28	0.14	0.01		LPM	−18	9 Mar	9.8E−4	0.28	0.07	44.64	
LGM	−20	9 Mar	1.3E−4	0.33	0.07	0.01		LPM	−25	9 Mar	1.6E−3	0.26	0.05	78.68	
LGM	−25	9 Mar	1.5E−4	0.34	0.07	0.01		LPM	−28	9 Mar	1.6E−3	0.25	0.01	84.79	
LGM	−30	9 Mar	1.8E−4	0.36	0.07	0.21		LPM	−32	9 Mar	1.6E−3	0.25	0.04	96.59	
LGM	−35	9 Mar	2.3E−4	0.35	0.14	2.93		LPM	−36.5	9 Mar	7.3E−4	n.a.	0.06	152.90	
LGM	−3	9 May	6.2E−5	0.30	2.94	0.02		LPM	−3	9 May	4.9E−5	n.a.	4.69	0.01	
LGM	−10	9 May	9.8E−5	0.32	0.10	0.01		LPM	−12	9 May	9.1E−5	n.a.	3.10	0.02	
LGM	−15	9 May	1.1E−4	0.33	0.13	0.24		LPM	−18	9 May	9.0E−4	0.26	0.05	45.29	
LGM	−20	9 May	1.6E−4	0.32	0.31	0.49		LPM	−25	9 May	1.5E−3	0.26	0.04	79.57	
LGM	−25	9 May	2.1E−4	0.32	0.13	1.19		LPM	−28	9 May	1.6E−3	0.27	0.06	87.42	
LGM	−30	9 May	2.3E−4	0.33	0.09	1.71		LPM	−32	9 May	1.4E−3	0.26	0.07	100.23	
LGM	−35	9 May	n.a.	0.33	0.17	1.97		LPM	−36.5	9 May	9.1E−4	0.21	0.12	134.90	
LGM	−3	9 Jun	n.a.	0.25	0.22	n.a.		LPM	−3	9 Jun	6.1E−5	0.25	3.60	0.01	
LGM	−10	9 Jun	1.5E−4	0.29	0.15	1.10		LPM	−12	9 Jun	1.1E−4	0.31	2.32	0.02	
LGM	−15	9 Jun	1.8E−4	0.31	0.12	1.03		LPM	−18	9 Jun	8.6E−4	0.31	0.07	39.05	
LGM	−20	9 Jun	2.7E−4	n.a.	n.a.	n.a.		LPM	−25	9 Jun	1.6E−3	0.28	0.04	84.23	
LGM	−25	9 Jun	3.0E−4	0.33	0.10	2.88		LPM	−28	9 Jun	1.6E−3	0.27	0.04	89.18	
LGM	−30	9 Jun	3.5E−4	0.31	0.11	3.68		LPM	−32	9 Jun	1.51E−3	0.27	0.04	106.66	
LGM	−35	9 Jun	4.0E−4	0.33	0.12	9.04		LPM	−36.5	9 Jun	6.4E−4	0.17	0.03	169.65	
LGM	−3	9 Sep	6.7E−5	0.25	0.14	0.01		LPM	−3	9 Sep	7.2E−5	0.29	5.97	0.01	293

LGM	−10	9 Sep	2.1E−4		0.91	3.05	294	LPM	−12	9 Sep	1.2E−4	0.37	6.88	0.02			
LGM	−15	9 Sep	2.9E−4	0.31	0.16	2.83		LPM	−18	9 Sep	9.7E−4	0.31	0.06	55.85			
LGM	−20	9 Sep	5.2E−4	0.31	0.13	6.57	289	LPM	−25	9 Sep	1.7E−3	0.28	0.08	89.10			
LGM	−25	9 Sep	5.5E−4	0.33	0.10	7.05	294	LPM	−28	9 Sep	1.7E−3	0.27	0.06	95.36			
LGM	−30	9 Sep	6.0E−4	0.31	0.09	7.29	294	LPM	−32	9 Sep	1.6E−3	0.26	0.03	109.32			
LGM	−35	9 Sep	6.1E−4	0.31	0.05	65.84	291	LPM	−36.5	9 Sep	8.6E−4	0.19	0.04	174.50			297

Concentrations of dissolved gases are in cm^3 STP l^{-1}; n.a.= not available.

(IV) a layer deeper than 30 m, characterized by a steep EC gradient (increasing from 0.8 to 1.6 mS cm^{-1}), indicating a significant modification of water chemistry. Layers I and II form the mixolimnion, which is characterized by cyclical water circulation. The EC gradients do not change over time in layers III and IV, suggesting that these layers are not involved in seasonal circulation of the lake waters.

[20] In warm months, the EC measured in LGM shows—in accordance with the recognized thermal stratification—three well-defined regions (Figures 2a and 2e). In contrast, during winter, the thermal stratification vanishes because the waters are completely mixed, which results in the EC being almost constant from the surface to the bottom of the lake (Figure 2e).

[21] The pH values in both lakes are highest in shallow waters; they are lowest during cold months (7.1 in LPM and 6.7 in LGM) and highest during summer (8.4 in both lakes). In LPM, the measured pH values are nearly constant from a depth of about 15 m until the bottom, although they varied over time within 0.7 pH units (Figure 2f). The bottom waters exhibited similar pH values in LGM and LPM (Figures 2f and 2g). Despite the pH profile differing between the two lakes, the similarity of recorded variations at both the surface and the bottom suggests that similar processes control the carbonate systems in the two lakes.

[22] In September 2008, September 2009, and October 2009, we carried out CTD profiles at different places on each lake. The locations of the sampling points are shown in Figure 1. These profiles strongly suggest the presence of horizontal continuity of temperature, EC, and pH at each depth in both LPM and LGM.

3.2. Water Chemistry of Monticchio Lakes

3.2.1. Major Elements

[23] The analysis of the lake waters revealed that the main cations in LPM and LGM waters are Ca, Mg, Na, K, and Fe, while the main anions are HCO_3, Cl, and SO_4 (Tables 1 and 2). According to previous investigations [e.g., *Chiodini et al.*, 1997; *Aguilera et al.*, 2000; *Kusakabe et al.*, 2008], HCO_3 is the main anion in the LPM water as well as in other crater lakes (i.e., Nyos and Monoun) and is also the main anion in the LGM water (Table 1). Nevertheless, we observed wide concentration ranges in both lakes. In LPM [Ca (21.4–51.7 ppm), Mg (12.9–29.1 ppm), Na (29.2–42.3 ppm), K (19.6–28.6 ppm), and Fe (106.3–243.6 6 ppm)] and in

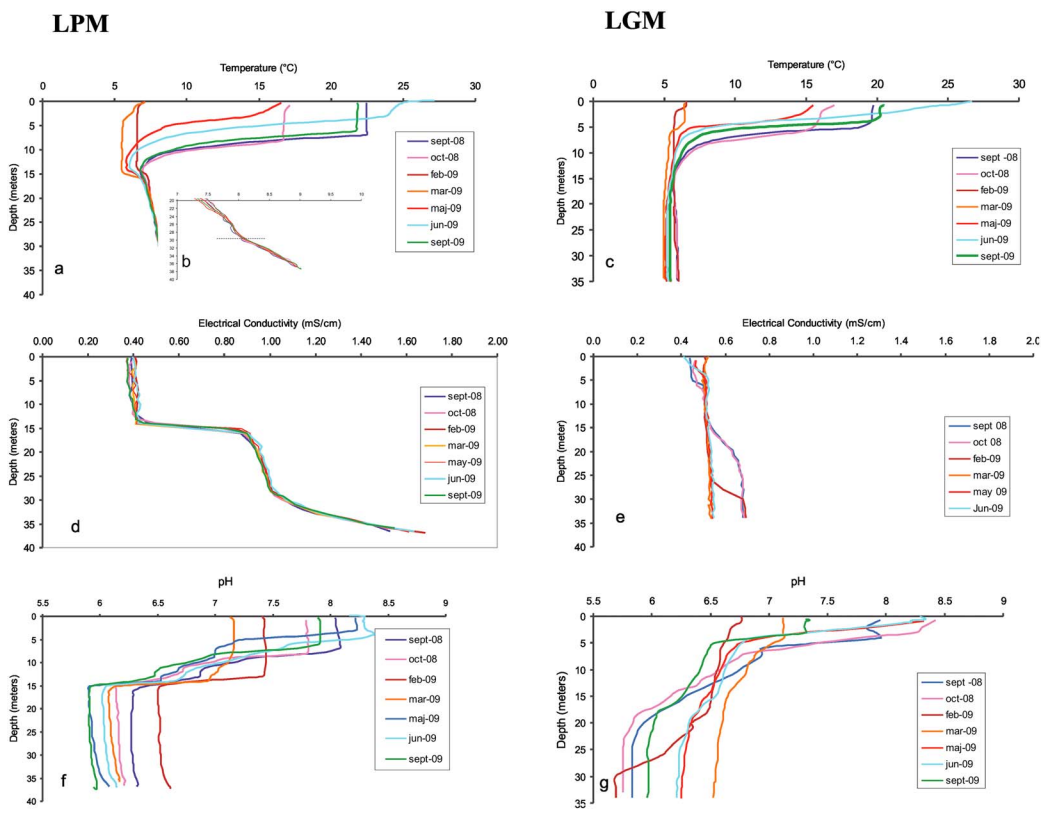

Figure 2. Profiles recorded with the CTD probe in the deepest point of LPM and LGM between September 2008 and September 2009. (a) Temperature in LPM. (b) Temperature at deeper than 20 m on an enlarged scale in LPM. (c) Electrical conductivity normalized to 20°C in LGM. (d) pH in LPM. (e) Temperature in LGM. (f) Electrical conductivity normalized to 20°C in LPM. (g) pH in LGM.

LGM: [Ca (25.7–42.5 ppm), Mg (8.653–11.452 ppm), Na (29.9–34.9 ppm), K (18.8–22.3 ppm), and Fe (0.6–1.7 ppm)]. There was marked variability with depth in both LPM and LGM.

[24] The overall relative concentrations of dissolved anions and cations measured in the lake waters are consistent with those of Mt. Vulture groundwaters (Figures 3a and 3b). This strongly suggests that similarly to the groundwater circulating in the region of the Mt. Vulture volcano [*Paternoster et al.*, 2010], the enrichment of ions dissolved in the waters of the lakes mainly derives from dissolution of local volcanic rocks. The high Fe and NH_4 levels distinguish the waters of the two lakes from groundwater (Tables 1 and 2) [*Paternoster et al.*, 2010), with the highest level in the LPM water deeper than 18 m. LPM exhibits a permanent chemical stratification, with the amount of dissolved solutes being lower in water shallower than 18 m. Below this depth, the relative concentrations of solutes are almost constant over time, supporting that the deep waters in LPM are stagnant. Therefore, the water chemistry coupled with the recorded physical-chemical parameters indicate that LPM is a meromictic lake with a well-defined monimolimnion at deeper than 18 m. LGM is characterized by a summer chemical stratification.

[25] Comparison of the data for Monticchio lakes with those for other CO_2-rich lakes highlights the low concentrations of Cl, Br, SO_4, and F in both LPM and LGM waters, suggesting that they are not directly fed by gases released from magma sited at a shallow depth (i.e., SO_2 and HCl), since sulfur degassing from basaltic melt becomes significant only in hydrothermal systems at lower pressures [*Spillart et al.*, 2006; *Metrich et al.*, 2010] and/or high temperatures [*Varekamp et al.*, 2000]. Recently, investigation on $\delta^{34}S$ of dissolved sulfate in Mt. Vulture groundwaters [*Paternoster et al.*, 2010] has highlighted that sulfur dissolved in Mt. Vulture groundwaters derives by leaching of volcanites, while the contribution from other sources can be neglected.

[26] The high Fe concentrations in LPM are in the range of values of other volcanic lakes (e.g., Momoun, Nyos) [*Kusakabe et al.*, 1989; *Aguilera*

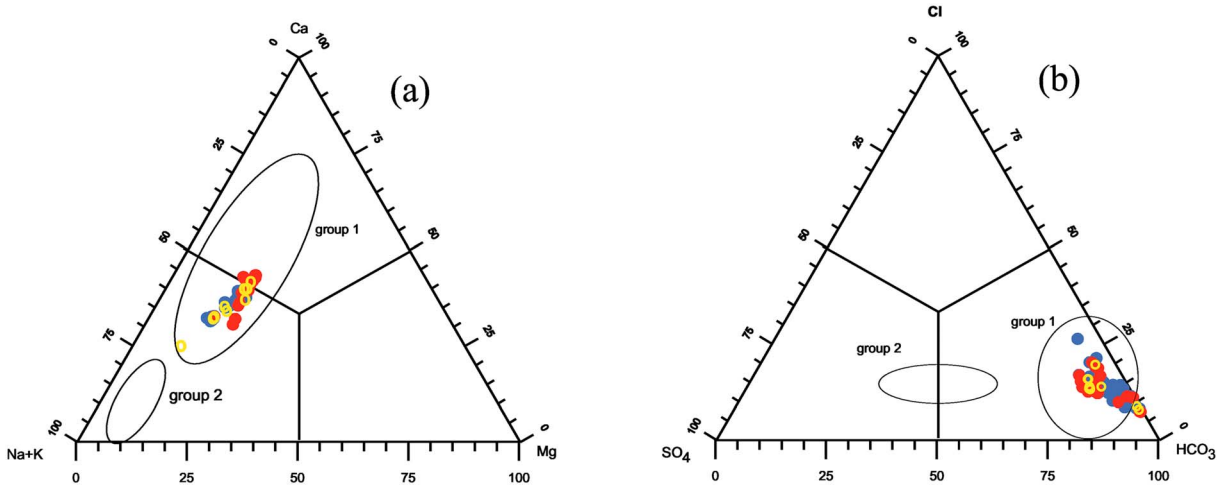

Figure 3. (a) Na + K-Ca-Mg ternary plot. (b) SO_4-Cl-HCO_3 ternary plot. Two distinct groups of groundwaters were distinguished in the region of Mt. Vulture: high salinity (group 1) and low-to-medium salinity (group 2) [*Paternoster*, 2005]. The waters of both lakes fall into the category of group 2 (Mt. Vulture low-to-medium salinity groundwater). Red circles, LPM samples; blue circles, LGM samples; yellow circles, samples from the channels.

et al., 2000; *Teutsch et al*., 2009]. However, such values are comparable with those from other meromictic lakes close to lignite mines [*Dietz et al*., 2012] and where the difference in Fe concentrations between monimolimnion and mixolimnion sustains the meromixis.

[27] The measured pH, Cl, and SO_4 levels highlight that Monticchio lakes fall into the category of "quiescent lakes" proposed by *Varekamp et al.* [2000], which is quite different from "CO_2-dominated lakes" (e.g., Nyos Lake) and active crater lakes (e.g., Mt. Ruapehu, New Zealand, and Yugama Lake, Japan).

3.2.2. Water Isotopic Composition: δD and $\delta^{18}O$

[28] Both lakes show isotopic variations of H and O with depth and time (Tables 1 and 2). In LPM, the isotopic signature of H and O is almost constant at depths below 25 m, and neither δD nor $\delta^{18}O$ data vary markedly over time, confirming the stagnant character of this layer. According to previous investigations [*Marini*, 2006], their isotopic compositions fall within the range of Mt. Vulture groundwater [*Paternoster et al*., 2008], supporting that groundwater flows into the lake below 25 m. In contrast, the isotopic compositions of shallow waters show a large variability, with δD and $\delta^{18}O$ ranging from −35‰ to −48‰ and from −4‰ to −8‰ (versus SMOW), respectively.

[29] As proposed by *Marini* [2006, and references therein], such observations indicate that the isotopic compositions of H and O of shallow waters of the two lakes are affected by seasonal variations. Moreover, according to literature data [*Marini*, 2006, and references therein], the δD and $\delta^{18}O$ values recorded between September 2008 and September 2009 are consistently less negative for the LGM than the LPM water column. Variations of the H and O isotopes with depth have been observed in LGM during summer, whereas their isotopic profiles show smaller variations with depth during winter.

[30] H and O isotopic ratios of the waters flowing through the channel connecting the two lakes is the same as that of LPM shallow waters during both winter and summer (Table 2). Analogously, no differences in δD and $\delta^{18}O$ were identified between the shallow waters of LGM and the water flowing out of the channel connecting that lake to the Ofanto River (Tables 1 and 2). The collected data corroborate the notion that water dynamics coupled to evaporation processes influence the H and O isotopic compositions over the entire water column of LGM [*Marini*, 2006, and references therein].

[31] According to previous studies [*Mongelli et al*., 1975; *Marini*, 2006, and references therein], the δD-versus-$\delta^{18}O$ diagram (Figure 4) indicates that LPM waters deeper than 25 m fall along the local meteoric water line (LMWL) [*Paternoster et al*., 2008], whereas LPM shallow waters and all LGM waters exhibit a linear trend, which is typical of evaporative processes (Figure 4) as in other volcanic lakes [e.g., *Varekamp and Kreulen*, 2000]. The slope of the evaporation line computed from

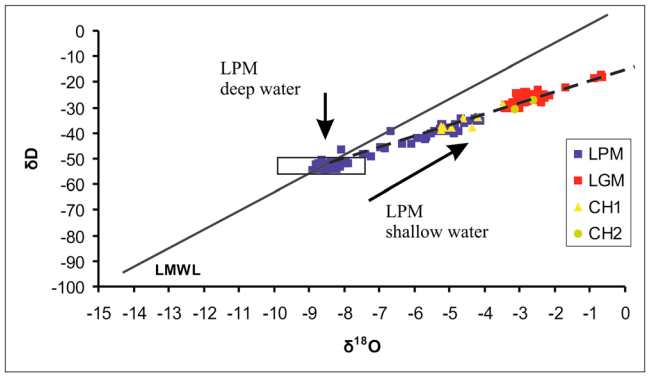

Figure 4. Plots of δD versus $\delta^{18}O$ for (blue squares) LPM and (red squares) LGM waters. Most of the samples fall on the evaporation line, dashed line ($y = 4.6x - 14.3$). The local meteoric water line (LMWL) is that defined by *Paternoster et al.* [2008]. Yellow squares indicate water samples of the channel between the two lakes, and green points indicate water samples from the LGM outflow channel. Open rectangle, δD. $\delta^{18}O$ of Mt. Vulture groundwater ($-60‰ < \delta D < 52‰$; $-10‰ < \delta^{18}O < -7.5‰$) from *Paternoster et al.* [2008].

our data set differs slightly from those proposed previously [*Mongelli et al.*, 1975; *Marini*, 2006], which is probably related to a more limited data set (~30 samples). In the present study, we computed the evaporation line based on 130 samples collected at LPM and LGM during 11 sampling fields between 2006 and 2010 [*Caracausi*, unpublished data; this work]. Such data allow us to better define the following equation for the evaporation line:

$$\delta D = 4.6\,\delta^{18}O - 14.3. \quad (1)$$

[32] Since the isotopic composition of groundwater is essentially the same as meteoric values [*Paternoster et al.*, 2008], we used linear regressions to evaluate the recharge altitudes of groundwater feeding LPM (isotopic value of rainfall versus altitude), as proposed by *Paternoster et al.* [2008]. Those authors, using data from *Mongelli et al.* [1975], estimated that the meteoric recharge altitude of LPM was about 1130 m above sea level (asl). The mean recharge altitudes estimated using our data are about 894 and 952 m for $\delta^{18}O$ and δD, respectively; therefore, the mean recharge altitude can be considered to be about 925 m (the Monticchio lakes are located at 660 m asl).

3.2.3. Total Dissolved Inorganic Carbon and CO_2

[33] The amount of DIC increases with depth and is comparable in both lakes from the surface down to a depth of 10 m (Tables 1 and 2). In this layer, values range between 3.1 and 6.6 mmol/L; below that depth, we observed different behaviors in the two lakes. In LGM, the increase with depth is slight and regular in winter time, and below 30 m, the amount ranges from 17.8 to 20.8 mmol/L, which is double that of samples at 25 m. In September and October 2008, the DIC concentration increased sharply below 20 m, reaching 31.5 mmol/L at the bottom. In February 2009, only at depths greater than 30 m were the DIC concentrations comparable with the values during September and October 2008. In LPM, below 10 m, the DIC concentrations increase sharply toward the lake bottom, reaching more than 1 order of magnitude higher than those in shallow waters (Table 2); below 20 m, they range from 22.9 to 41.3 mmol/L.

[34] The chemical stratification of LPM is clearly revealed by the $\delta^{13}C_{DIC}$ profiles (Table 2 and Figure S1 in the supporting information)[1]; between the surface and 18 m, the values, which range from −1.4‰ to −5.16‰, vary with depth and time. Below 20 m, these profiles are within the uncertainties, and the values increase from −2.3‰ to −0.2‰ at the bottom. This provides further evidence that this zone of the lake is not affected by seasonal variations.

[35] Between depths from approximately 0 to 20 m, LGM is characterized by $\delta^{13}C_{DIC}$ values that range widely, from −4.2‰ to −2.4‰ (Table 1 and Figure S1 in the supporting information). According to DIC profiles, in May and June 2009, $\delta^{13}C_{DIC}$ did not show significant variation with depth. In contrast, the $\delta^{13}C_{DIC}$ values in September 2009 increase up to −2.4‰ in the bottom water (Table 1 and Figure S1 in the supporting information).

All supporting information may be found in the online version of this article.

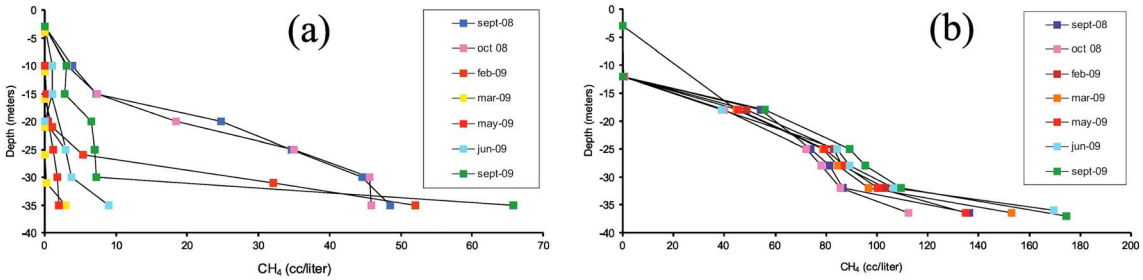

Figure 5. Profiles of CH_4 dissolved in the (a) LGM and (b) LPM waters.

[36] The high DIC in deep waters of both lakes could be related to the inflow of CO_2-rich groundwater into their deep portions.

[37] The $\delta^{13}C$ values of the DIC measured in bottom samples from both lakes do not fall within the typical organogenic range, instead lying closer to the range of values measured in the magmatic fluids of Italian volcanoes [e.g., *Allard*, 1987], thus suggesting a mainly magmatic origin of the carbon species dissolved in the water. Furthermore, according to a study of other Italian volcanic lakes by *Caliro et al*. [2008], the more negative values for LGM are probably due to a CO_2 contribution from organic sources in that lake and/or the amount of DIC generated by organic matter oxidation.

[38] We also computed the concentration of CO_2 dissolved in the waters of both lakes (Tables 1 and 2) based on the dissolved carbonate equilibrium [*Stumm and Morgan*, 1996]. The equilibrium in solution among inorganic carbon species $H_2CO_3^* = H_2CO_3 + CO_{2(aq)}$, $H_2CO_3^-$, and CO_3^{2-} is related to the pH, temperature, and DIC amount. The P_{CO2} values in the shallower water of both lakes, calculated by using the Henry's law constant and calculated $H_2CO_3^*$ by applying carbonate equilibrium equations, are extremely low, ranging from 0.001 to 0.01 atm (Tables 1 and 2). Below 20 m, the values increase and are higher in LPM than in LGM. Our results highlight that CO_2 [given as $H_2CO_3^* = H_2CO_3 + CO_{2(aq)}$] is the main carbon species and is dissolved in large amounts in the bottom waters of both lakes, suggesting that CO_2 is added mainly at the bottom of the Monticchio lakes. However, according to *Caracausi et al*. [2009], the dissolved CO_2 represents only a small fraction of the possible highest possible CO_2 solubility for LPM and LGM.

3.3. Dissolved Gases

[39] According to *Caracausi et al*. [2009], the waters of the Monticchio lakes are rich in dissolved CO_2 and CH_4 (Table 3). The concentrations of dissolved CH_4 increase with depth, suggesting it mainly comes from sediments. A biogenic origin of CH_4 has been suggested by *Caracausi et al*. [2009] based on the $\delta^{13}C_{CH4}$ values (ranging between −60.0‰ and −61.8‰ versus PDB); this is also supported by the δD of CH_4 [*Caracausi*, unpublished data].

[40] The two lakes exhibit different CH_4 concentration profiles. The CH_4 dissolved along the LGM water column varies over time (Figure 5a) as a function of the dynamics of the lake water. This strongly supports the recorded variations of the physical-chemical parameters and chemical isotopic compositions of water. During September and October 2008, the CH_4 concentrations increased sharply below 10 m. The waters were enriched in CH_4 from the bottom (45.9–48.6 cm^3 STP L^{-1}) up to a depth of ~10 m (3.9–3.1 cm^3 STP L^{-1}), which is orders of magnitude higher than in the shallower waters (up to 3 m deep).

[41] The CH_4 dissolved in LGM waters decreased significantly in February 2009 down to 25 m, while its concentration remained high close to the bottom (Figure 5a and Table 3). Then, in May 2009, the CH_4 concentration declined sharply along the water column to 2.0 cm^3 STP L^{-1} at a depth of 34 m. The dissolved CH_4 gradually increased during subsequent months, starting from the bottom water (Figure 5a).

[42] In contrast, the concentration gradient of CH_4 in the LPM water column does not show substantial variations over time (Figure 5b). The concentrations of CH_4 dissolved in the bottom water range between 112.5 and 174.5 cm^3 STP L^{-1}, and such values are consistently higher than those for LGM bottom water. CH_4 is present in trace amounts from a depth of about 12 m up to the surface.

[43] The amount of dissolved O_2 dramatically decreases in the LPM monimolimnion and below a depth of 10 m in LGM (Table 3), suggesting that anoxic conditions dominate at greater depths.

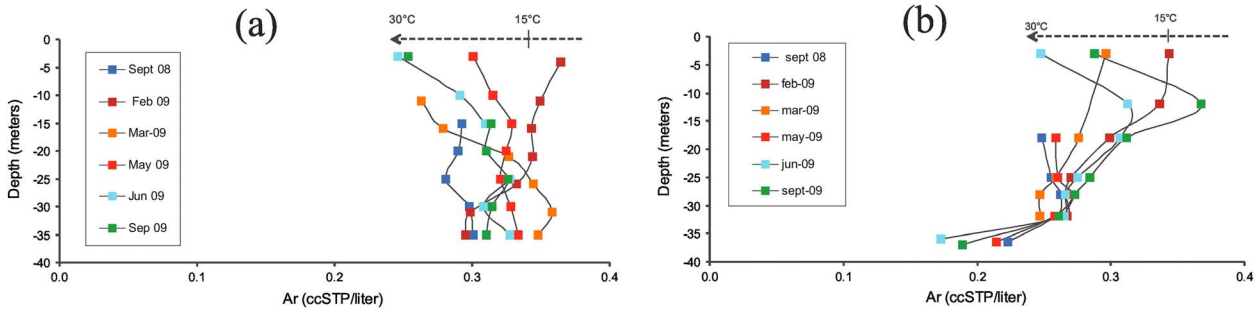

Figure 6. Profiles of Ar dissolved in the (a) LGM and (b) LPM waters.

Moreover, the occurrence of O_2-rich and CH_4-poor waters in shallower layers in both lakes suggests that the CH_4 concentration was reduced by oxidation in shallow waters.

[44] A complete mixing of the waters takes place once a year in LGM, while the concentrations of O_2 is below the values of air-equilibrated water (6.4 cm^3 STP L^{-1}) and is almost constant over time, suggesting that processes of O_2 consumption develop rapidly in that lake.

[45] The Ar concentration in LPM is lowest in the bottom waters. The values fall within a narrow range, from 0.17 and 0.22 cm^3 STP L^{-1}, and are higher in the shallower layer. The concentration profiles are within the uncertainties ($\pm$0.1 cm^3 STP L^{-1}) between 25 and 32 m. In the shallower layer, the concentrations of Ar dissolved in the lake waters vary markedly over time. Considering that the average temperature of groundwater recharging in the Mt. Vulture area is 12°C [*Parisi*, 2009], Ar dissolved in LPM deep waters displays values well below its equilibrium with the atmosphere (Figure 6b). In contrast, the variation recorded in the shallow water is consistent with seasonal variations of the air temperatures (Figure 6b), indicating that surface waters are equilibrated with atmospheric Ar.

[46] The amount of Ar dissolved in the surface waters of LGM is also consistent with equilibration with air (Figure 6a). Nevertheless, the Ar concentration profiles with depth vary over time according to water circulation in the lake.

[47] At all depths, the $^{40}Ar/^{36}Ar$ isotopic ratio ranges from 289 to 297 in both lakes (Table 3), which clearly indicates an atmospheric origin of Ar [*Ozima and Podosek*, 2002]. This finding, coupled to the Ar concentration in the bottom water being lower than that of waters in equilibrium with atmosphere, strongly suggests that these waters have been affected by degassing processes and losing part of the initial dissolved Ar.

[48] Significant contributions of nonatmospheric He have been observed in the Monticchio lakes [*Caracausi et al.*, 2009]. The He dissolved in LPM and LGM waters consistently exceeds that for equilibrium with air. Its amount strongly varies over time in LGM and constantly increases toward the lake bottom (Figure 7a), suggesting it enters the lake at the bottom. The He concentration increases progressively during summer in LGM waters, reaching its highest measured gradient between shallow and deep waters in September 2008. During the following winter, the amount of dissolved He decreased dramatically and then began to increase again during the subsequent seasonal warming (Figure 7a).

[49] He is an inert noble gas, and hence, only physical processes or additional inputs can modify its concentration in LGM waters. Thus, the sharp decrease in He in winter is due to a complete overturning of the water, and despite some He being lost to the atmosphere, the LGM waters maintain He concentrations above equilibrium with air also during winter (Figure 7a and Table 3). It is noteworthy that the observed seasonal modification of the dissolved He in the LGM water column is analogous to that of CH_4, indicating that dissolved gases strongly constrain the LGM water dynamics.

[50] One striking feature of the He dissolved in LPM water is that its concentration increases from the bottom toward a depth of about 28 m, as do Ar concentrations, then decreases toward the surface down to values that exceed those expected for equilibrium with air (Figure 7b and Table 3). The concomitant increases in He and Ar from the bottom of the lake toward a depth of 28 m are not the result of degassing during sampling, since this trend was highly reproducible.

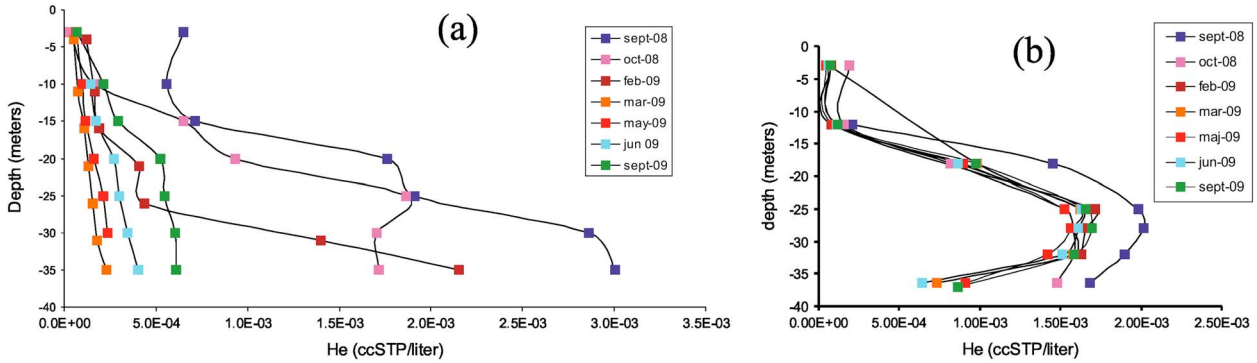

Figure 7. Profiles of He dissolved in the (a) LGM and (b) LPM waters.

[51] The presence of noble-gas anomalies in a lake could be related to specific processes of gas exchange between ascending bubbles and water flowing into the lake [*Holzner*, 2008; *Holzner et al.*, 2012] or an inflow at 28 m of groundwater He-rich and with Ar concentrations lower than water in equilibrium with atmosphere.

[52] Consider the following observations: (1) When using a fish finder, we did not observe bubble plumes or the release of bubbles from the bottom of the lake close to the sampling point; (2) dissolved CH_4 concentration markedly decreases from the lake bottom toward a depth of 28 m at LPM, displaying almost homogeneous concentration gradients over time and over a long period of observation, with no variations with depth of the carbon isotopic composition of methane in the LPM monimolimnion, highlighting that oxidation processes cannot explain the variation of CH_4 concentrations in deep water [*Caracausi*, unpublished data]; (3) there are strong variations at the same depth of both the temperature and the electrical conductivity of LPM water; and (4) there is less Ar in the deeper water than in the water in equilibrium with the atmosphere as well as in water from springs and wells of the Mt. Vulture region, which are affected by degassing processes during water circulation [*Costa*, 2010; *Caracausi*, unpublished data]. From these observations, it is reasonable to assume that at a depth of about 28 m, there is an injection of groundwater that is colder and richer in noble gases than that entering at the bottom of the lake, with the amounts of noble gases being modified by degassing processes (gas saturation condition due to $P_{gas} > P_{hydrostatic}$), occurring during groundwater circulation before its injection into the lake.

[53] The isotopic ratio of He together with the He/Ne ratio of gases dissolved in deep waters of both lakes [*Caracausi et al.*, 2009] clearly indicates a mantle origin of He dissolved in the Monticchio lakes. The highest ratio, of 6.1 Ra (Ra being the $^3He/^4He$ ratio in atmosphere, of 1.39×10^6), was measured at LPM in July 2006 [*Caracausi et al.*, 2009]. This is indistinguishable from those measured in the fluid inclusions of olivine found in LPM explosion ejecta [*Martelli et al.*, 2008; *Caracausi et al.*, 2013].

[54] The amount of tritium in the two lakes is generally less than 2 TU (Tables 1 and 2) and is consistent with the values measured in rain samples and groundwater of the Mt. Vulture area [*Fuganti and Sigillito*, 2008]. Assuming that tritium decay annually produces about 4.5 10^{-12} cm^3 STP L^{-1} of ^3He, the contribution of tritiogenic ^3He is negligible.

4. Processes Governing Lake Water Chemistry

4.1. Evaporation: δD Versus [Cl^-]

[55] The O and H isotopic data indicate that LPM is fed by groundwater entering the monimolimnion, while evaporation modifies the isotopic composition of the lake water down to a depth of 25 m (Figure 4 and Table 2). In contrast, evaporation affects the H and O isotopic compositions of the entire LGM water column (Figure 4 and Table 1). The increase in the ionic concentration is inversely proportional to the volumetric residual fraction of evaporating water [equation (2)]. Therefore, in order to better describe the processes related to evaporation and considering that chemical processes (i.e., dissolution and/or precipitation) can reasonably act in the lake waters, we investigated variations of Cl—a conservative ion that does not participate markedly in geochemical and biochemical processes—together with those of water isotopes following *Nicolosi* [2010].

[56] The volumetric residual fraction and Cl^- are related according to

$$[Cl^-] = [Cl_0^-]/f \quad (2)$$

[57] where $[Cl^-]$ is the Cl^- concentration at the end of each evaporative step, $[Cl_0^-]$ is the initial Cl^- concentration, and f the volumetric residual fraction of water.

[58] In isotopic modeling of evaporation, we used δD rather than $\delta^{18}O$, since the latter could interact with the significant CO_2 content in the waters of the Monticchio lakes. In accordance with *Nicolosi* [2010], we adopted the *Craig and Gordon* [1965] and *Gonfiantini* [1986] approach, whereby the evaporation from a free water surface into the atmosphere can be described by the variation of the isotopic composition of an evaporating water body as

$$\delta = \left(\delta_0 - \frac{A}{B}\right) f^B + \frac{A}{B} \quad (3)$$

where δ and δ_0 are the final and initial isotopic compositions of the water body, respectively; f is the volumetric residual fraction of the water; and

$$A = \frac{h\delta_a + \varepsilon k + \frac{\varepsilon}{\alpha}}{1 - h + \varepsilon k} \quad (4)$$

$$B = \frac{h - \varepsilon k - \frac{\varepsilon}{\alpha}}{1 - h + \varepsilon k} \quad (5)$$

where h is the atmospheric relative humidity ($0 \le h \le 1$), δ_a is the isotopic composition of atmospheric moisture, εk is the kinetic isotopic enrichment factor, and α is the fractionation factor [where $\varepsilon = (\alpha - 1) \times 1000$].

[59] A mean annual relative humidity of 0.8 (i.e., 80%) was used [*Nicolosi*, 2010]; however, a variation in the relative humidity of 10% does not markedly affect the computation results. According to *Nicolosi* [2010], the δ_a values were estimated based on the assumed isotopic equilibrium between atmospheric moisture and precipitation [*Gibson et al.*, 2008, and references therein] as

$$\delta_a = \frac{\delta_p - \varepsilon}{\alpha} \quad (6)$$

where δ_p is the isotopic value of precipitation. The εk value (in per mil) can be evaluated using the relationships reported by *Gonfiantini* [1986]: εk (^{18}O) = 14.2(1 − h) and εk (H) = 12.5(1 − h).

[60] Previous investigations [*Mongelli et al.*, 1975] indicated that the evaporative process of LPM shallow waters that flow through the channel connecting the two lakes continue in LGM, so firstly tested this model. Groundwater is the starting water of our model because it feeds the lakes, and the following values of groundwater were used: δD = −54‰; Cl = 0.52 meq/L [e.g., *Celico and Summa*, 2004; *Paternoster et al.*, 2008]. As discussed above, the δD value (−54‰) represents the intersection between the regression line of lake waters and the local meteoric water line (LMWL) (Figure 4). Water from a well (PM well) near the lakes (~300 m from LPM and LGM) has a mean chloride concentration of 0.52 meq/L, which is in accordance with data of springs and water in the area [*Paternoster*, 2005; *Parisi*, 2009]. The fixed value of chloride (0.52 meq/L) was also chosen considering that evaporating water of epilimnion has values always over this value (± 0.01). As shown in Figure 8b, starting from groundwater composition, a simple evaporation is not able to produce most of LPM shallow water values, but also LGM shallow waters cannot derive from the simple process of groundwater evaporation or LPM shallow water evaporation.

[61] Therefore, in accordance with *Nicolosi* [2010], we need to set up a more complex theoretical model to explain the δD and Cl^- concentrations in the shallow waters of both Monticchio lakes.

[62] Water evaporation in both lakes mainly occurs in the epilimnion where waters are well mixed and chemically homogeneous. A box model was applied to the chemical and isotopic balances of the epilimnions of the Monticchio lakes (see Figure S2 in the supporting information) while considering the main inflows and outflows.

[63] The groundwater outflow does not affect δD and $[Cl^-]$ values, and hence, it can be neglected. As noted by *Schettler and Albéric* [2008], a high percentage of the precipitation undergoes evapotranspiration instead of draining, and considering that the amount of rain that falls onto the surfaces of the Monticchio lakes is always less than 2.7% of the epilimnion volume [*Nicolosi*, 2010], the contribution from precipitation can be neglected since it would only influence the final estimations within data errors. Thus, the balances of the Monticchio lakes are simplified because only groundwater inflow and evaporation need to be considered.

[64] Our model takes into account that the epilimnion is characterized by continuous groundwater

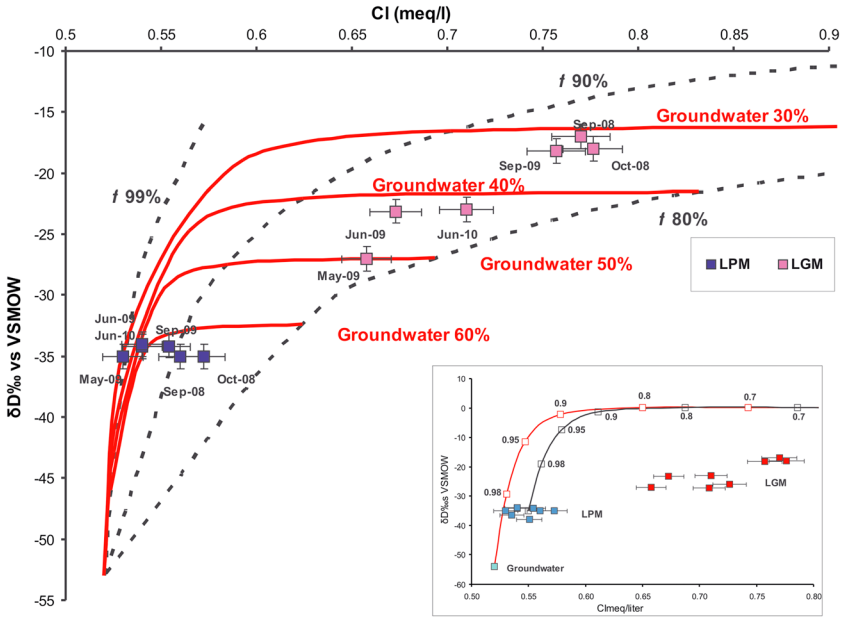

Figure 8. Lines representing steps of evaporation of the lake water and subsequent mixing of the residual water with groundwater. (a) All the percentage values are referred to the volume, which essentially represents the epilimnion. Each red line shows the theoretical steady state values for the same groundwater inflow (e.g., 30%, 40%, 50%, and 60%) and different residual fractions (f values); these lines result from the successive mixing of two components for Cl^- and δD obtained for progressive residual fractions (e.g., 0.1, 0.2, and 0.3) by equations (2) and (3) of the groundwater inflow (fixed percentage), up to the steady state. Each dashed black line shows the theoretical steady state values for the same residual fraction (i.e., 80%, 90%, and 99%) and different groundwater inflows; each line results from the successive mixing of two components for a fixed residual fraction and progressive groundwater inflow. (b) Plot of δD versus $[Cl^-]$; the groundwater was fixed at δD = −54‰ and $[Cl^-]$ = 0.52 meq/L; the values of LPM and LGM are referred to shallow waters (at a depth of ~3 m). The red and black lines represent the trends of the water values during evaporation starting from the groundwater and the shallow water of LPM, respectively. The numbers along the curves indicate the residual fraction of water f for theoretical evaporation. The error bar for each δD value (±1‰) appears within the corresponding symbol.

inflow and evaporation (outflow), with the consequence that the final chemical and isotopic values are reached when these two components are in a steady state dynamic balance. The calculation is based on a succession of steps of water evaporation from the epilimnion and the addition of new groundwater to the residual water. The values of Cl^- and δD from the evaporation process are computed by equations (2) and (3), while the addition of groundwater to the residual lake water is expressed by a binary mixing equation, i.e.,

$$[Cl^-] = [Cl^-]_{(gro)} \cdot (x) + [Cl^-]_{(res)} \cdot (1 - x) \qquad (7)$$

where $[Cl^-]_{(gro)}$ is the concentration of Cl^- in groundwater, (x) is the fraction of groundwater (in percentage), and $[Cl^-]_{(res)}$ is the Cl concentration in residual water after evaporation, and

$$\delta D = \delta D_{(gro)} \cdot (x) + \delta D_{(res)} \cdot (1 - x) \qquad (8)$$

where $\delta D_{(gro)}$ is the deuterium isotopic ratio in groundwater, (x) is the fraction of groundwater (in percentage), and $\delta D_{(res)}$ is the deuterium isotopic ratio in evaporation residual water.

[65] Each simulation reached steady state values that can be roughly considered to be the expected theoretical values of both the evaporation and the addition of groundwater for epilimnion water. The observed δD and $[Cl^-]$ values of almost all shallow waters of both lakes (up to a depth of at least ~3 m) fall within plausible ranges for the obtained theoretical values of both evaporation and groundwater inflow (Figure 8a).

[66] Plotting the data on a calculated theoretical grid (Figure 8a) reveals that the groundwater inflow in LPM is highest (above 60%) during periods of highest evaporation (in September and October, with a relatively low residual fraction; f ~ 90%). The groundwater inflow (30%–40%) and evaporation (97%–99%) are relatively low in May and June. It is noteworthy that the values for September 2008 and September 2009 are similar (within the error bar), as are those for June 2009 (Figure 8a),

suggesting a seasonal character for both evaporation and groundwater inflow. However, unfortunately, curves for the groundwater contributions for LPM prevent an accurate evaluation of the relative groundwater inflow because of data similarity.

[67] The residual fraction of evaporating water from LGM does not change much over time, always falling within the range of 81%–88%. The obtained results also show that the groundwater inflow exhibits a seasonal variability between 30% and 50%. Moreover, these values were very similar in September 2008, June 2009, and September 2009.

[68] Our calculations show that the groundwater inflow is greater for LPM than for LGM; in contrast, the latter has a mean evaporative rate greater than LPM. The different characteristics of the two lakes could reasonably explain the great variability of the chemical and isotopic (H and O) compositions of LGM waters than that for LPM waters. Moreover, our results also show that LGM shallow waters receive a large contribution from groundwater, corroborating the inference of groundwater inflow into LGM. Hence, LPM shallow water flowing through the channel connecting the two lakes is not the main water inflow into LGM, unlike what was previously believed [*Mongelli et al.*, 1975; *Chiodini et al.*, 2000; *Celico and Summa*, 2004]. The greater surface area of LGM is responsible for the great effect of evaporation at LGM than at LPM.

4.2. Precipitation and Dissolution of Carbonate Minerals

[69] Solutes dissolved in LPM and LGM are controlled by both chemical reactions and water mixing as the consequence of overturning or the inflow of groundwater, and/or diffusive process through the waters. The different behaviors of solutes dissolved in the shallower waters of both lakes suggest evidence that the water chemistry is altered by precipitation or dissolution of minerals. Therefore, with the aim of verifying if such mineralogical species are involved in these processes in the two lakes, we calculated the saturation indexes of the mineral species based on the water chemical composition and physical-chemical parameters (temperature and pH).

[70] The saturation index values (SI = log IAP/KS, where SI is the saturation index, IAP is the ion activity product, and KS is the solubility product constant) were calculated by using PHREEQC (version 2.15.0) equilibrium geochemical speciation mass transfer computer program [*Parkhurst and Appelo*, 1999]. Taking into account that the Monticchio lakes are rich in gases and the strong influence of the CO_2 concentration on water-gas-rock interactions, the SI values were calculated using pH values coupled to HCO_3 and the calculated CO_2 from carbonate equilibrium equations. The results suggested that the water chemistry is modified by precipitation (i.e., carbonate minerals). The SI values (see Figure 3 in the supporting information) indicate that calcite and dolomite are systematically oversaturated in the shallow waters of both lakes only during summer, when the pH values increase (Figure 2) reasonably due to photosynthesis, but tend to be undersaturated in deep waters. Both siderite and pyrite are oversaturated in the deeper permanently stratified layer of LPM. The SIs in the deep stratified water volume of LPM are strongly related to the redox conditions and the dissolved CO_2. A previous investigation of the geochemistry of sediment found both pyrite and siderite in the sediment [*Schettler and Alberic*, 2008], and hence, the chemistry of deeper LPM waters is controlled by the stability of minerals and the inflow of CO_2. In contrast, carbonate species and sulfur in LGM deep water are undersaturated ($SI < 0$). It is noteworthy that the SIs for which mineral decrease with increasing depth, further illustrating the key role played by changes in pH due to the presence of CO_2.

5. Water Density and Characteristics of the Monticchio Lakes

[71] The mixing processes of different vertically stacked water volumes in a lake are driven by differences in density between contiguous water volumes. Density is, in turn, a function of temperature, dissolved solutes, and gases, so any changes in these variables with depth in a lake will induce a density gradient along the water column.

[72] *Cioni et al.* [2006] evaluated the water density in LPM based on temperature and dissolved solids and found that the water density of the LPM monimolimnion is higher than that of the shallow water. Nevertheless, this conclusion was based on data collected at a single sampling time. Based on our data set and according to the approach outlined by *Boehrer and Schultze* [2008], we calculated the density of LPM waters and that of LGM waters between September 2008 and September 2009. The water density was computed using the temperature, solutes, and dissolved gases. Our results are

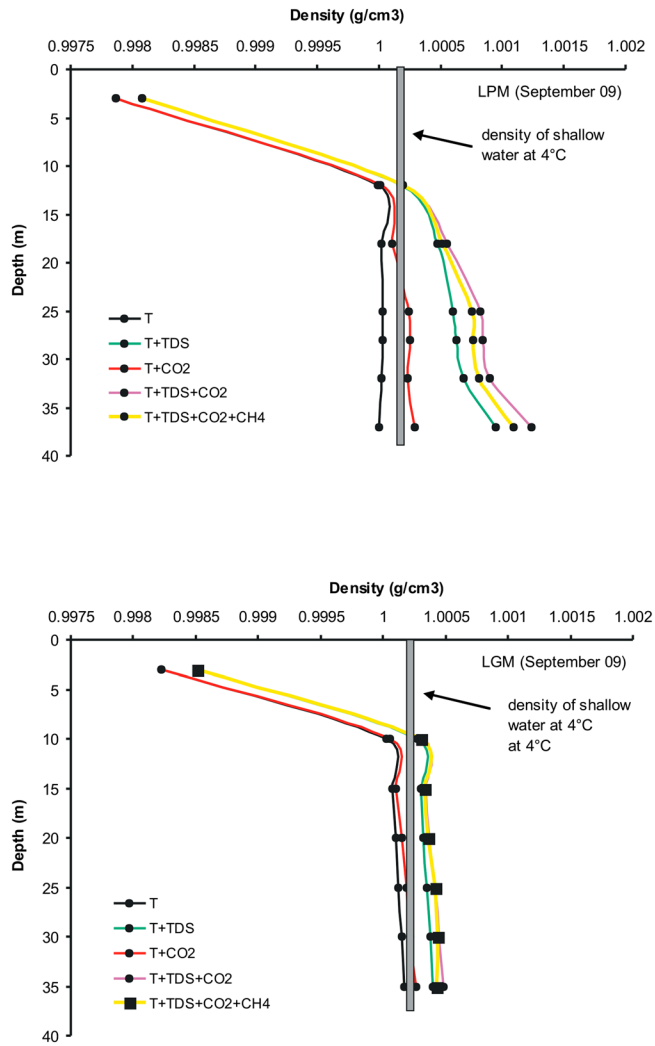

Figure 9. Plots of water density versus depth for (a) LPM and (b) LGM in September 2009. The strip around the value of 1.0002 g cm^{-3} indicates the density of shallow water at 4°C. In winter, the average air temperature in the Mt. Vulture area (at the Melfi meteorological station) is typically 4°C–5°C [*Nicolosi*, 2010]. The air temperature is probably lower at the Monticchio lakes (660 m asl) than at Melfi station (located at 580 m asl). Although we have no data for the winter months, continuous records obtained during the period from 29 May 2010 to 6 June 2010 confirm such behavior [*Nicolosi*, 2010] and indicate that the mean daily air temperature above the Monticchio lakes is 2°C lower than that measured at Melfi station (18.2°C and 20.3°C, respectively). Nevertheless, considering the high specific heat of water (fourfold higher than that of air) and that lake waters are subject to radiant heating by sunlight, we can expect the shallow-water temperature to be higher than the air temperature. Therefore, during the cold months, the mean temperature of the shallow waters of the Monticchio lakes can be expected to exceed 4°C. Dissolved CH_4 exerts a destabilizing effect, since the water density is reduced by its low molar mass and relatively high partial molar volume. The stabilizing effects of dissolved solutes and CO_2 are greater than the destabilizing effects of temperature and dissolved CH_4.

in good agreement with previous investigations [*Cioni et al.*, 2006, and references therein], confirming that the density of LPM shallow water is lower than that of deep water during both summer (September 2009) and winter (Figure 9). In contrast, there are well-defined variations of density with depth in LGM only during summer (i.e., September 2009; Figure 9).

[73] In particular, Figure 9 highlights that dissolved solutes and CO_2 exert major effects on the increase in density with depth in both lakes. In summer, when the concentrations of gases dissolved in the deep water of the two lakes are comparable, density calculations produce discrepant values. Hence, it is evident that dissolved solutes are mainly responsible for the differences in densities between the

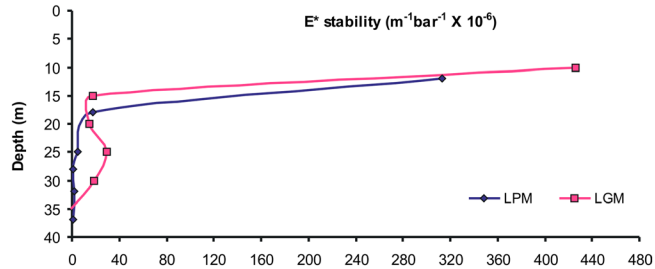

Figure 10. Distribution of the local water-column stability with depth modified for the effects of dissolved gas (E^*, see text) in LPM and LGM. The plotted data refer to September 2009.

two lakes. In particular, the higher concentrations of Fe and Mn (which have high molar masses) in LPM water compared to those in LGM water mainly determine the different densities in the two lakes, at least during warm months.

[74] The variations of both water and gas chemistry in the shallow waters of the two lakes do not modify the density appreciably over time, so cooling of these waters (Figure 9) would increase their density enough to mix LPM waters down to a depth of about 12 m (i.e., in February 2009). The density of LPM shallow waters at 4°C is always lower than that of the monimolimnion, thereby avoiding any mixing with deep waters. In contrast, the density of LGM shallow water at 4°C is close to the values of the hypolimnion (Figure 9), and furthermore, the lake has a different bathymetry, displaying an average depth of only 12 m; hence, a low-energy event, such as a low wind speed, could trigger mixing. CTD data together with that of water and gas chemistry revealed that mixing of shallow waters occurs during the coldest period of the year, indicating that temperature plays a key role in the mixing of the Monticchio lakes, but that its efficacy with depth varies between the two lakes.

[75] In contrast to *Schettler and Albéric* [2008], we found no evidence that LGM is dimictic. Our geochemical investigations instead indicate that it is a warm monomictic lake and support previous conclusions about LPM, which is a meromictic lake, where mixing only involves shallow waters [*Cioni et al.*, 2006, and references therein].

6. Stability of the Monticchio Lakes

[76] The overall lake stability represents the energy required to mix the lake waters to a nearly uniform density. We evaluated the stability along water columns of the Monticchio lakes during the warm period (September 2009)—when the deep waters of both lakes are enriched with gas—by means of classical methods and using the calculated water densities. Gas exsolution is able to destroy the local stability. The CO_2 concentration exhibits two behaviors: (i) in undersaturated conditions, it increases the water density and stabilizes deep layers (as discussed above); and (ii) if P_{CO2} exceeds the ambient hydrostatic pressure, the exsolution can trigger a turnover [*Kling et al.*, 2005]. The proposed formulation [*Kling*, 1988; *Kling et al.*, 1994] takes into account the degree of gas saturation as follows:

$$E* = \left[\left(\frac{1}{\rho}\right)\left(\frac{d\rho}{dz}\right)\right] \times \left[\left(\frac{P_{\mathrm{amb}}}{P_{\mathrm{gas}}}\right) - 1\right] \times \left(\frac{1}{P_{\mathrm{gas}}}\right) \quad (9)$$

where E^* is the local stability (in m^{-1} bar^{-1}), ρ is the density, z is the depth (in m), and P_{amb} and P_{gas} are the ambient hydrostatic pressure and the dissolved-gas pressure (in bars), respectively. The first term is the standard oceanographic definition of local stability. The second and third terms need to be included to account for the nonlinear effects of dissolved gases on the density of lake water and to distinguish between conditions where the gas saturation may be present in a layer of low absolute gas pressure (e.g., near the lake surface). Negative and positive values of E^* indicate unstable and stable conditions, respectively [*Kling*, 1988; *Kling et al.*, 1994].

[77] The E^* values for the Monticchio lakes in September 2009 are plotted in Figure 10. For both lakes, it is evident that the stability is high in layers with the highest density gradient (between the surface layer and the layer at a depth of 10–15 m). Both lakes have positive local stability, except for LGM bottom waters, where the E^* values are close to zero, denoting a possible local instability. Taking into account the gas pressure (sum of partial pressure of dissolved gases), the local stability (E^* value) of LPM (which is richer in dissolved gases in LGM) decreases dramatically because the waters are close

to the level where exsolution occurs, especially those near the bottom of the lake (Figure S4 in the supporting information). The gases dissolved in LGM are far from the exsolution line (Figure S4 in the supporting information) due to the periodic mixing that gradually releases the gases accumulated in deep waters to the surface, and the stability increases mainly due to the high molar mass and relatively low partial molar volume of dissolved CO_2. Our data confirm the significant role of dissolved gases in determining the stability of lake water.

[78] Gas oversaturation can be easily reached in LPM by a forced ascent of deep waters to a shallow depth (with a lower hydrostatic pressure) as a consequence of processes such as landslides, earthquakes.

[79] There are historical reports [*Tata*, 1778; *Palmieri and Scacchi*, 1852; *Ciarallo and Capaldo*, 1995] of the occurrence of gas outbursts from both Monticchio lakes back to no later than about 200 years ago. Moreover, those events recurred over and over again from both lakes between 1810 and 1820. According to *Caracausi et al.* [2009] it is also reasonable to expect that dangerous outgassing phenomena could happen again in the future at the Monticchio lakes, whether caused by CO_2 accumulation in the crust [*Chivas et al.*, 1987] or by outgassing of CO_2-oversaturated magma, since its presence at depth (in or below the continental crust) cannot be ruled out.

7. Conclusions

[80] To our knowledge, this is the first report of geochemical investigations of the two Monticchio lakes covering 1 year of observations. A large vertical difference in density in the LPM water column and its invariability should be responsible for the immiscibility of shallow and deep water volumes. Furthermore, the nearly constant values of almost all investigated parameters at deeper than 14 m corroborates the meromictic character of LPM. In contrast to previous reports [*Schettler and Albéric*, 2008] which classified classifying LGM as a warm monomictic lake, we observed complete overturning of the water in winter 2009 and a subsequent new chemical stratification during spring 2009.

[81] We have shown that δD and Cl are powerful parameters to evaluate the groundwater supply and water evaporation processes in lakes. By the use of a new conceptual model of water balance, we found that groundwater inflow is greater for LPM than for LGM. LGM displays a mean evaporative rate greater than that for LPM. We have also revealed that LPM water entering LGM through the connecting channel represents only a portion of the total recharge to LGM. This lake is also fed by sublacustrine groundwater inflow in contrast to previous investigations [*Celico and Summa*, 2004].

[82] According to its meromictic character, LPM is capable of a greater accumulation of both TDIC (about 4 times that of LGM) and dissolved gases, especially in deep waters. The differences in water dynamics between the two lakes lead to the dissolved gases accumulated in the deep waters of LPM being double those of LGM.

[83] In spite of a clear mantle signature of He isotopes (up to 6.1 Ra), the low concentrations of typical volcanic components and the measured pH, Cl, and SO_4 levels indicate the lack of direct transport of fluids from degassing magma seated at shallow depth, although the presence of degassing melt at great pressure cannot be ruled out.

[84] Our results have provided clear evidence that He, together with other noble gases, is useful not only as a geochemical tracer for indicating the magmatic origin but also for improving our understanding of the dynamics of lake water and tracing recharge of groundwater to the lake. A groundwater recharge model is proposed to explain the observed layered structure of the noble gases in LPM. The main injection of noble-gas-rich groundwaters into the lake occurs at a depth of about 28 m, and in addition, there is a minor injection of groundwaters with a low concentration of noble gases at the bottom.

[85] Our results support those of previous studies [*Chiodini et al.*, 2000; *Cioni et al.*, 2006; *Caracausi et al.*, 2009], indicating that the total pressure of gases dissolved at different depths would be maintained far from the saturation condition if both the dynamics and supply of gases in the two Monticchio lakes will not change in the future.

[86] Finally, we would like to stress that applying a combined limnological-geochemical approach produces a better understanding of and constraints to the dynamics of two maar lakes formed during the last activity of the Mt. Vulture volcano. These lakes represent a singular case of twin lakes showing very different recharging, physical structures, and dynamics, although they also show some similarities. Such knowledge allows historical records to be used to identify the processes underlying gas

releases,and provides new scientific tools to assess future possible gas hazards.

Acknowledgments

[87] We appreciate comments and suggestions of J. Tyburczy (Editor), C. Evans, M. Kusakabe, and J. C. Varekamp, which contribute to improving this paper.

References

Aeschbach-Hertig, W., R. Kipfer, M. Hofer, D. M. Imboden, R. Wieler, and P. Signer (1996), Quantification of gas fluxes from the subcontinental mantle: The example of Laacher See, a maar lake in Germany, *Geochim. Cosmochim. Acta*, *60*, 13–41.

Aguilera, A., G. Chiodini, R. Cioni, M. Guidi, L. Marini, and B. Raco (2000), Water chemistry of lake Quilotoa (Ecuador) and assessment of natural hazards, *J. Volcanol. Geotherm. Res.*, *97*, 271–285.

Allard, P. (1987), Endogenous magma degassing and storage at Mt. Etna, *Geophys. Res. Lett.*, *24*, 2219–2222.

Allen, J. R. M., et al. (1999), Rapid environmental changes in southern Europe during the last glacial period, *Nature*, *400*, 740–743.

Assayag, N., D. Jézéquel, M. Ader, E. Viollier, G. Michard, F. Prévot, and P. Agrinier (2008), Hydrological budget, carbon sources and biogeochemical processes in Lac Pavin (France): Constraints from $\delta^{18}O$ of water and $\delta^{13}C$ of dissolved inorganic carbon, *Appl. Geochem.*, *23*, 2800–2816.

Bishop, P. K. (1990), Precipitation of dissolved carbonate species from natural waters for $\delta^{13}C$ analysis—A critical appraisal, *Chem. Geol.*, *80*, 251–259.

Boehrer, B., and M. Schultze (2008), Stratification of lakes, *Rev. Geophys.*, *46*, RG2005, doi:10.1029/2006RG000210.

Brauer, A., J. Mingram, U. Frank, C. Günter, G. Schettler, S. Wulf, B. Zolitchka, and J. F. W. Negendank (2000), Abrupt environmental oscillations during the Early Weichselian recorded at Lago Grande di Monticchio, Southern Italy, *Quat. Int.*, *73*(74), 79–90.

Caliro, S., G. Chiodini, G. Izzo, C. Minopoli, A. Signorini, R. Avino, and D. Granieri (2008), Geochemical and biochemical evidence of lake overturn and fish kill at Lake Averno, Italy, J. Volcanol. Geotherm. Res., *178*, 305–316.

Caracausi, A., P. M. Nuccio, R. Favara, M. Nicolosi, and M. Paternoster (2009), Gas hazard assessment at the Monticchio crater Lakes of Mt. Vulture, a volcano in Southern Italy, *Terra Nova*, *21*, 83–87, doi:10.1111/j.1365-3121.2008.00858.x.

Caracausi, A., M. Martelli, P. M. Nuccio, M. Paternoster, and F. M. Stuart (2013), Active degassing of mantle-derived fluid: A geochemical study along the Vulture line, Southern Apennines (Italy), *J. Volcanol. Geotherm. Res.*, *253*, 65–74, doi:10.1016/j.jvolgeores.2012.12.005.

Celico, P., and G. Summa (2004), Idrogeologia dell'area del Vulture (Basilicata), *Boll. Soc. Geol. Ital.*, *123*, 343–356.

Chiodini, G., R. Cioni, M. Guidi, L. Marini, C. Principe, and B. Raco (1997), Water and gas chemistry of the Lake Piccolo of Monticchio (Mt. Vulture, Italy), *Current Research on Volcanics Lakes*, Newsletter of the IAVCEL Commission on Volcanic Lakes, edited by S. J. Freth, *10*, 3–8.

Chiodini, G., R. Cioni, M. Guidi, G. Magro, L. Marini, and B. Raco (2000), Gas chemistry of Lake Piccolo of Monticchio, Mt Vulture, in December 1996, *Acta Vulcanol.*, *12*(1–2), 139–143.

Chivas, A. R., I. Barnes, W. C. Evans, J. E. Lupton, and J. O. Stone (1987), Liquid carbon dioxide of magmatic origin and its role in volcanic eruptions, *Nature*, *326*, 587–589.

Ciarallo, A., and L. Capaldo (1995), *Journey to Vulture, Comments on Tenore and Giussone's Travel Diary (1838)*, Edizioni Osanna Venosa, Venosa (in Italian).

Cioni, R., L. Marini, and B. Raco (2006), Il lago Piccolo di Monticchio: geochimica dei fluidi e valutazione del rischio di eruzione limnica in *La Geologia del Monte Vulture, Regione Basilicata*, edited by C. Principe, pp. 171–177.

Cosenza, P., G. Riccobono, A. Caracausi, and M. Nicolosi (2008), Campionatore di profondità per gas disciolti, *Rapporti Tecnici INGV*, *66*, 1–8.

Cosenza, P., G. Riccobono, A. Caracausi, M. Nicolosi, and M. Nuccio (2012), Campionatore per T.D.I.C. per acque profonde, *Rapporti Tecnici INGV*, *221*, 1–9.

Costa, M. (2010), Degassamento profondo nell'area del Monte Vulture (Basilicata): Rilevanza, processi che lo governano e sua origine, Master's thesis, Univ. di Palermo.

Craig, H., and L. I. Gordon (1965), Deuterium and oxygen-18 variations in the ocean and the marine atmosphere, in *Proceedings of a Conference on Stable Isotopes in Oceanographic Studies and Paleotemperatures*, edited by E. Tongiorgi, pp. 9–130, Spoleto, Italy.

Delmelle, P., and A. Bernard (2000), *Encyclopedia of Volcanoes*, edited by H. Sigurdsson, pp. 877–895, Academic, San Diego, Calif.

Dietz, S., D. Lessmann, and B. Boherer (2012), Contribution of solutes to density stratification in a meromictic lake (Waldsee/Germany), *Mine Water Environ.*, *31*, 129–137, doi:10.1007/s10230-012-0179-3.

Epstein, S., and T. Mayeda (1953), Variation of $\delta^{18}O$ content of water from natural sources, *Geochim. Cosmochim. Acta*, *4*, 213–224.

Fuganti, A., and V. Sigillito (2008), Characteristic, origins, and age of the water from springs and wells on the Monte Vulture (Basilicata Region, Italy), *Ital. J. Eng. Geol. Environ.*, 47–70 doi:10.4408/IJEGE.2008-02.O-04.

Gambardella, B., C. Cardellini, G. Chiodini, F. Frondini, L. Marini, G. Ottonello, and M. V. Zuccolini (2004), Fluxes of deep CO_2 in the volcanic areas of central-southern Italy, *J. Volcanol. Geotherm. Res.*, *136*, 31–52, doi:10.1016/j.jvolgeores.2004.03.018.

Gibson, J. J., S. J. Birks, and T. W. D. Edwards (2008), Global prediction of δA and δ^2H-$\delta^{18}O$ evaporation slopes for lakes and soil water accounting for seasonality, *Global Biogeochem. Cycles*, *22*, BG2031, doi:10.1029/2007GB002997.

Giggenbach, W. F. (1990), Water and gas chemistry of Lake Nyos and its bearing on the eruptive process, *J. Volcanol. Geotherm. Res.*, *42*, 337–362.

Gonfiantini, R. (1986), Environmental isotopes in lake studies, in *Handbook of Environmental Isotopes Geochemistry*, vol. *3*, edited by P. Fritz, and J. C. Fontes, pp. 113–168, Elsevier, New York.

Gunkel, G., C. Beulker, B. Grupe, and F. Viteri (2008), Hazards of volcanic lakes: analysis of Lakes Quilotoa and Cuicocha, Ecuador, *Adv. Geosci.*, *14*, 29–33.

Holzner, C. P. (2008), Noble gases as tracers for mixing and gas exchange processes in lakes and oceans, Diss. ETH Zurich, No. 17757, pp. 1–101.

Holzner, C. P., Y. Tomonaga, A. Stöckli, N. Denecke, and R. Kipfer (2012), Using noble gases to analyze the efficiency of artificial aeration in lake Hallwill, Switzerland, *Water Resour. Res.*, *48*, 1–8, doi:10.1029/2012WR012030.

Igarashi, G., M. Ozima, J. Ishibashi, T. Gamo, H. Sakai, Y. Nojiri, and T. Kawai (1992), Mantle helium flux from the bottom of Lake Mashu, Japan, *Earth Planet Sci. Lett.*, *108*, 11–18.

Kendall, C., and T. B. Coplen (1985), Multisample conversion of water to hydrogen by zinc for stable isotope determination, *Anal. Chem.*, *57*, 1437–1440.

Kling, G. W. (1987), Seasonal Mixing and Catastrophic Degassing in Tropical Lakes, Cameroon, West Africa, *Nature*, *237*, 1022–1024.

Kling, G. W., M. A. Clark, H. R. Compton, J. D. Devine, W. C. Evans, A. M. Humphrey, E. J. Koenigsberg, J. P. Lockwood, M. L. Tuttle, and G. N. Wagner (1987), The 1986 lake Nyos Gas disaster in Cameroon West Africa, *Science*, *236*, 169–175.

Kling, G. W. (1988), Comparative transparency, depth of mixing, and stability of stratification in lakes of Cameroon, West Africa, *Limnol. Oceanogr.*, *33*, 27–40.

Kling, G. W., W. C. Evans, M. L. Tuttle, and G. Tanyileke (1994), Degassing of Lake Nyos, *Nature*, *368*, 405–406.

Kling, G. W., W. C. Evans, G. Tanyileke, M. Kusakabe, T. Ohba, Y. Yoshida, and J. V. Hell (2005), Degassing Lakes Nyos and Monoun: defusing certain disaster, *Proc. Natl. Acad. Sci.*, *102*, 14,185–14,190.

Kusakabe, M., T. Ohsumi, and S. Aramaki (1989), The lake Nyos disaster: chemical and isotopic evidence in waters and dissolved gases from three Cameroonian lake, Nyos, Monoum and Wum, *J. Volcanol. Geotherm. Res.*, *39*, 167–185.

Kusakabe, M., Y. Nojiri, and M. Narita (1990), A simple plastic syringe sampler for in situ fixing of the total CO_2, dissolved in lake water, Int. Working Group Crater Lakes Newsl., *2*, 11–14.

Kusakabe, M., G. Z. Tanyileke, S. A. McCord, and S. G. Schladow (2000), Recent pH and CO_2 profiles at Lakes Nyos and Monoum, Cameroon: implications for the degassing strategy and its numerical simulation, *J. Volcanol. Geotherm. Res.*, *97*, 241–260.

Kusakabe, M., M. Ohba, Y. Issa, H. Satake, T. Ohizumi, W. C. Evans, G. Tanyileke, and G. W. Kling (2008), Evolution of CO_2 in lakes Monoun and Nyos, Cameroon, before band during controlled degassing, *Geochem. J.*, *42*, 93–118.

Marini, L. (2006), Le caratteristiche isotopiche delle acque sotterranee del Monte Vulture e delle acque dei Laghi di Monticchio, in *La Geologia del Monte Vulture*, edited by C. Principe, pp. 149–154, Regione Basilicata.

Martelli, M., P. M. Nuccio, F. M. Stuart, V. Di Liberto, and R. M. Ellam (2008), Constraints on mantle source and interactions from He-Sr isotope variation in Italian Plio-Quaternary volcanism, *Geochem. Geophys. Geosyst.*, *9*, Q02001, doi:10.1029/2007GC001730.

Métrich, N., A. Bertagnini, and A. Di Muro (2010), Conditions of magma storage, degassing and ascent at Stromboli: New insights into the volcano plumbing system with inference on the eruptive dynamics, *J. Petrol.*, *51(3)*, 603–626.

Mongelli, F., C. Panichi, and E. Tongiorgi (1975), Studio termico ed isotopico dei crateri-laghi di Monticchio (Lucania), *Arch. Oceanogr. Limnol.*, *18*, 167–188.

Nagao, K., M. Kusakabe, Y. Yoshida, and G. Tanyileke, (2010), Noble gases in Lakes Nyos and Monoun, Cameroon, *Geochem. J.*, *44*, 519–543.

Nicolosi, M. (2010) The Monticchio crater lakes: fluid geochemistry and circulation dynamics, PhD thesis, Univ. of Palermo, Palermo, Italy.

Nojiri, Y., M. Kusakabe, K. Tietze, J. I. Hirabayashi, H. Sato, Y. Sano, H. Shinohara, T. Njine, and G. Tanyileke (1993), An estimate of CO_2 flux in Lake Nyos, Cameroon, *Limnol. Oceanogr.*, *38*(4), 739–752.

Nuccio, P. M., A. Paonita, A. Rizzo, and A. Rosciglione (2008), Elemental and isotope covariation of noble gases in mineral phases from Etnean volcanics erupted during 2001–2005, and genetic relation with peripheral gas discharges, *Earth Planet Sci. Lett.*, *272*, 283–290, doi:10.1016/j.epsl.2008.06.007.

Ozima, M., and F. A. Podosek (2002), *Noble Gas Geochemistry*, 286 pp., Cambridge Univ. Press, Cambridge.

Palmieri, L., and A. Scacchi (1852), *The volcanic region of Mount Vulture and the earthquake that took place there on August 14th 1851*, Printing Office Gaetano Nobile, Naples, Italian, pp. 160.

Parisi, S. (2009) Hydrogeochemical tracing of the groundwater flow pathways in the Mount Vulture volcanic aquifer system (Basilicata, southern Italy). PhD thesis, Univ. of Basilicata, Potenza, Italy.

Parkhurst, D. K. L., and C. A. J. Appelo (1999), *PHREEQC, Guide to a computer program for speciation batch –reaction, one dimensional transport, and inverse geochemical calculations*, *U.S. Geol. Surv. Water Resour. Invest. Rep.*, *99-42559*, 31,299.

Pasche, N., M. Schmid, F. Vazquez, C. J. Schubert, A. Wüest, J. D. Kesssler, M. A. Pack, W. S. reeburgh, and H. Bürgmann (2011), Methane sources and sinks in Lake Kivu, *J. Geophys. Res.*, *116*, G03006, doi:10.1029/2011JGOO1690,2011.

Paternoster, M. (2005), Mt. Vulture volcano (Italy): a geochemical contribution to the origin of fluids and to a better definition of its geodynamic setting. PhD thesis, Univ. of Palermo, Palermo, Italy.

Paternoster, M., M. Liotta, and R. Favara (2008), Stable isotope ratios in meteoric recharge and groundwater at Mt, Vulture volcano, southern Italy, *J. Hydrol.*, *348*, 87–97, doi:10.1016/j.jhydrol.2007.09.038.

Paternoster, M., S. Parisi, A. Caracausi, R. Favara, and G. Mongelli (2010), Groundwaters of Mt. Vulture volcano, southern Italy: Chemistry and isotope composition of dissolved sulphate, *Geochem. J.*, *44*, 125–135.

Sano, Y., H. Wakita, T. Oshsumi, and M. Kusakabe (1987), Helium isotope evidence for magmatic gases in lake Nyos, Cameroon, *Geophys. Res. Lett.*, *14*, 1039–1041.

Sano, Y., M. Kusakabe, J. Hirabayashi, Y. Nojiri, H. Shinohara, T. Njine, and G. Tanyileke (1990), Helium and carbon fluxes in lake Nyos Cameroon: Constrain on next gas burst, *Earth Planet Sci. Lett.*, *99*, 303–314.

Schettler, G., and P. Albéric (2008), Laghi di Monticchio (Southern Italy, Region Basilicata): Genesis of sediments—A geochemical study, *J. Paleolimnol.*, *40*(1), 529–556, doi:10.1007/s10933-007-9180-4.

Spilliaert, N., N. Métrich, and P. Allard (2006), S-Cl-F degassing pattern of water-rich alkali basalt: modelling and relationship with eruption styles on Mount Etna volcano, *Earth Planet Sci. Lett.*, *248*, 772–786, doi:10.1016/j.epsl.2006.06.031.

Stumm, W., and J. J. Morgan (1996), *Aquatic Chemistry, Chemical Equilibria and Rates in Natural Waters*, John Wiley, New York, 3rd edition, pp. 1022.

Tata, D. (1778), *Letter about Mount Vulture addressed to his Excellency D. Guglielmo Hamilton, Knight of the Royal*

Order of "Bagno," His Britannic Majesty's Envoy and Minister Plenipotentiary at the Court of Naples, 62 pp., Simoniaca Printing Office, Naples (in Italian).

Teutsch, N., M. Schmid, B. Müller, A. N. Halliday, H. Bürgmann, and B. Wehrli (2009), Large iron isotope fractionation at the oxic-anoxic boundary in Lake Nyos, *Earth Planet.Sci. Lett.*, *285*, 52–60, doi:10.1016/j.epsl.2009.05.044.

Varekaamp, J. C., and R. Kreulen (2000), The stable isotope geochemistry of volcanic lakes, with examples from Indonesia, *J. Volcanol. Geotherm. Res.*, *97*, 309–327.

Varekamp, J. C., G. B. Pasternack, and G. L. Rowe Jr. (2000), Volcanic lake systematics: II. Chemical constraints, *J. Volcanol. Geotherm. Res.*, *97*, 161–179.

Zhang, S. R., X. X. Lu, H. G. Sun, J. T. Han, and D. L. Higgitt (2009), Major ion chemistry and dissolved inorganic carbon cycling in a human-disturbed mountainous river (the Luodingjiang River) of the Zhujiang (Pearl River), China, *Sci. Total Environ.*, *407*, 2796–2807, doi:10.1016/j.scitotenv.2008.12.036.

Zito, G., and F. Mongelli (1980), Thermal structure of a lake with water in vertical motion, *Nuovo Cimento C*, 3, 654–670.